Universidad
Carlos III de Madrid

UNIVERSITY DEGREE IN BIOMEDICAL ENGINEERING

ACADEMIC YEAR 2017-2018

BACHELOR THESIS:

"THEORETICAL AND NUMERICAL CHARACTERIZATION OF DEGASSED - DRIVEN FLOWS FOR BIOMICROFLUIDICS APPLICATION"

María Royo Cano

Tutors
Javier Rodríguez - Rodríguez
Pablo Peñas López

Leganés, 2018

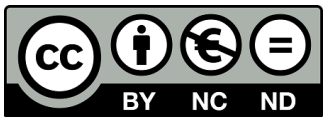

ABSTRACT

Biomedical microelectromechanical systems (BioMEMS) and Lab on a chip (LOC) devices represent very promising emerging technologies in the healthcare field due to their revolutionary outcomes. They include technologies operating for biological or biomedical purposes which are built from nano and micro scale fabrication techniques. This provides them characteristics such as portability, low cost per test, more sensitivity in detection mechanisms and, therefore, a reduction in sample processing times and efforts. However, there are still many challenges to face in the BioMEMS and LOC fields, such as the fact of controlling flows of fluids in microchannels or making these devices portable, as they usually need large and bulky pumping devices, which is a problem when trying to use them as Point-Of-Care (POC) or in developing countries. Flow control is very important for many applications in BioMEMS or LOC areas. There are cases in which the fluid velocity needs to be precisely controlled like, for instance, to mix fluid samples, to generate concentration gradients or even to avoid cells disruption due to high shear stresses. This is why over the lasts decades continuous and increasing research is being performed to find the most suitable fluid pumping mechanisms for each application.

In this project a not-so-well explored vacuum-driven pump is presented. The performance of the pump is based on the polydimethylsiloxane (PDMS) gas solubility or permeability, which makes this material suitable as a suction-driven pump, since when vacuumed PDMS is put in touch with air, sucks it from its surroundings, generating a negative pressure for driving fluid in microchannels. PDMS is a biocompatible, low cost, flexible polymer commonly used in BioMEMS and LOC devices due to its attractive characteristics. The physical description of the PDMS pump working mechanism is provided and a simulating tool based on the Finite Elements Method (FEM) has been developed to facilitate the PDMS pumps design depending on the application. In order to validate the open source software used as the solver of the differential equation underlying the pumping mechanism, it's results have been contrasted with the analytical solution to the problem and the numerical one obtained through Finite Differences. Then, numerical solutions for 2D and 3D geometries have been obtained in order to study different geometric effects in the pumping laws and show the potential of the tool, designed for the Microfluidics Research team in Universidad del País Vasco to perform a further research process regarding the PDMS as a pump.

Key words: BioMEMS; LOC; Flow control; Vacuum-driven pump; PDMS

ACKNOWLEDGEMENTS

Firstly, I am very grateful to my tutor, Javier Rodríguez-Rodríguez, for all his dedication, and my co-tutor, Pablo Peñas López, for his collaboration. I consider having learned a lot from their knowledge. Besides, I would like to thank the microfluidics research team in Universidad del País Vasco, who were looking for a detailed physical description of the PDMS pumping mechanism and opened this research line, for their collaboration and attention, specially when visiting them in Vitoria.

I would also like to thank my classmates and very close friends Raquel, Andrea, Luna and Rocío, which have been going through the same as I, for all their help. Apart from sharing many good times, we have all been supporting each other during the whole degree and have always been together, without them university would have not been the same.

I would also like to express my gratitude to Nacho, my boyfriend, for this patience and support in the most stressful moments.

Finally, I would really like to thank my family, specially my grandparents, for their encouragement and for being the proudest people of me I know. I would like to express here all my love to them.

CONTENTS

LIST OF FIGURES

LIST OF TABLES

1. INTRODUCTION

1.1. Objective

The reason why this project is being developed is to, in collaboration with the microfluidics research team in Universidad del País Vasco (UPV), study the viability of the not-so-well explored pumping mechanism based on the polydimethylsiloxane (PDMS) gas solubility and permeability.[1][2] PDMS is a polymer very used for BioMEMS manufacturing with characteristics such as biocompatible, low cost, flexible and, the most remarkable for this project, gas soluble and permeable. The objective of the study is the physical characterization of degassed PDMS as a pump in microfluidic systems. The pump consists on a previously degassed PDMS slab to which air diffuses, therefore, generating a negative pressure in a microfluidic channel able to drive the flow of microfluidics inside the system; being the main advantages of this pumping performance power free, easy to use and modular.[2]

There are two main objectives in the project, to physically describe and understand the underlying mechanism of gas pumping using PDMS (diffusion pumping) and to develop a tool to provide to the team in Vitoria that, in an easy and practical way, allows them to perform simulations of the pumping performance for different PDMS geometries and, hence, be able to study the viability of this pumping mechanism though the design of different PDMS pumps and further characterization after experimental validation of the numerical solutions. They are very interested in optimizing designs to achieve different pumping curves: constant rate, high rate even during a shorter time, etc. Each application may require a different pumping law, thus their interest of having such a software tool available.

The scheme followed in the thesis consists in first explaining the physics including a model of the problem and an extension of the model to cylindrical coordinates and a more complex fully three-dimensional geometry; then the numerical method to solve it, the Finite Element Method (FEM), since it is a partial differential equation (PDE) solver which allows to deal with complex geometries, and finally, the software used to implement it (FreeFem++) including why it has been chosen (free and multiplatform) and details and particularities of how it works.

A description of the pressure-driven flow of water generated along time through a circular channel is provided by modeling the gas diffusion in PDMS (described by the heat equation) and fluid flow in sequential steps for different geometries with

the FEM.

Since one main goal of the work is to use free tools available, FreeFem++ has been chosen as the FEM solver tool, and the open-source package GMSH to generate 3D meshes and use them later in FreeFem++. In order to validate this software as the simulating tool of the pump performance, the analytical solution to the problem has been computed in 1D but also a numerical solution through finite differences for the spatial discretization and the ODE (Ordinary Differential Equation) set for the time marching 1D has been obtained (implemented in Matlab), to be contrasted with the 1D FEM solution obtained with FreeFem++. Afterwards, 2D and 3D numerical solutions have been obtained for different geometries; solutions which will need to be validated with experimental results in order to characterize the PDMS performance as a pump for different applications.

1.2. Overview and motivation

1.2.1. BioMEMS, LOC devices and μTAS

Biomedical microelectromechanical systems or BioMEMS are used for delivery or analysis of biological and chemical. They have become an important subset of microelectromechanical systems (MEMS) systems since the 1970s and can belong to the fields of biology, medicine, engineering, materials science, chemistry, physics, clinical science, surgery, etc. having applications in genomics, proteomics, point-of-care diagnosis, tissue engineering, implants, etc.[3] BioMEMS overlap with both lab-on-a-chip (LOC) and micro total analysis systems (μTAS) and are sometimes synonymous with them. BioMEMS are more focused on fabrication techniques which allow biological applications,[3] while LOC devices on integrating laboratory processes and experiments in chips,[4] and μTAS on chemical analyses and may not include biological applications.[5] Controlling the flows of the samples is essential in order to reach the purposes for which BioMEMS, LOC and μTAS are designed.

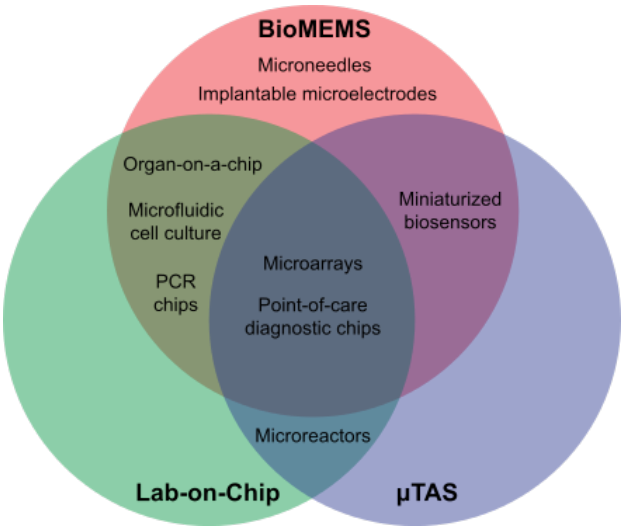

Fig. 1.1. Venn diagram that contrasts BioMEMS, LOC and μTAS.[6]

1.2.2. The small scale

The small dimensions either in BioMEMS, LOC or μTAS provide advantages over traditional systems at larger scales: the small-scale benefit itself, the high-throughput benefit and the quantitative one.[7] For BioMEMS:

- The **small-scale benefit** refers to the miniaturization of small units and to the fact that due to the small dimensions, the micromechanical parts are less sensitive to external vibrations and disturbances, the less energy they require to operate and the faster they react. Examples of small units are microfluids and cells; microfluids can be controlled and, thus, generate desired conditions such as determined concentration gradients or flows; and cells can be spatially or temporally monitored.[7] This benefit, therefore, allows basic or fundamental understanding of both cell mechanics and fluid flow at the microscale.

- The **high-throughput benefit** is obtained in fabrication techniques costs (in miniaturization techniques, mass production costs are similar to single production ones, which reduces single unit costs) and in experimental research, since operation and monitorization of many units can be simultaneously performed and, therefore, both statistical data obtained and costs decreased. BioMEMS allow to probe and image single cells in large numbers, which provides information about variability of cell behaviour, cell expression or even cell-cell communications, which is quite relevant in applications such as LOC biosensing systems or engineered tissue scaffolds.[7]

- The **quantitative benefit**: due to the small dimensions of the systems, quantitative predictions can be easily performed. Regarding fluids, this is allowed

due to their deterministic behaviour in microchannels, since at small dimensions, low Reynolds numbers govern the flows, providing laminar behaviours; and regarding cells, when reducing the scale, both cell density and cells spacing parameters can be controlled independently, while at macroscale not. These characteristics allow to make models even before fabrication steps.[7]

These benefits enable improvements in research and in lowering costs, which are key factors for BioMEMS, LOC and μTAS development.[3][4][5]

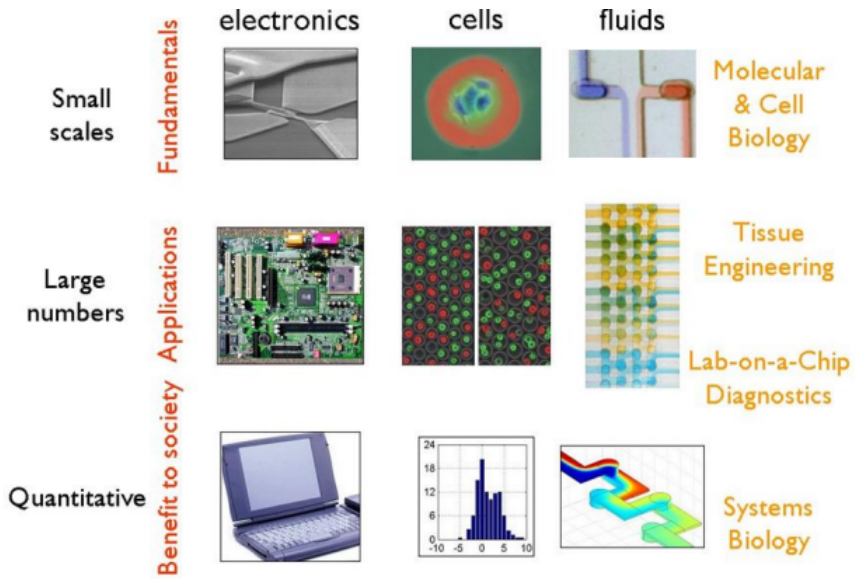

Fig. 1.2. The small scale benefit in microelectromechanical systems.[7]

However, when dealing with fluids, the small dimensions have also their drawbacks. Filling microfluidics channels is difficult because of the surface forces even if the fluid has a very low viscosity;[7] moving fluids inside microchannels and doing it in a controlled manner is also a challenge;[7][1][2] and even mixing them as well, due to their laminar behaviour.[7]

Besides, it is important to fill the channels completely, so avoiding air traps is required in order to facilitate the flows.[7] Bubbles are hydrophobic and their presence in microfluidic channels makes the flow even more difficult. In PDMS-based microdevices, removing them is one of the main needs as PDMS inert nature is hydrophobic by itself and flows are yet hard to generate.[1]

1.2.3. Main pumping mechanisms in microfluidics

There exist different mechanisms to drive the flow through the microchannels, being the main ones:

- **Pressure driven flows**
  - **Syringe pumps**: Are extremely precise but need power.
  - **Gravity pumps**: Consist of reservoirs set at a certain height.[8]

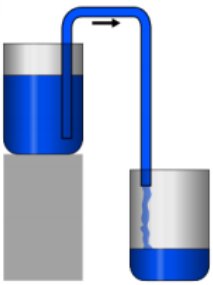

Fig. 1.3. Gravity pump.

  - **Surface tension-driven pumps**: Consists on placing two droplets with different radius at the ends of a microchannel and use the pressure difference from their surface tensions.[9]

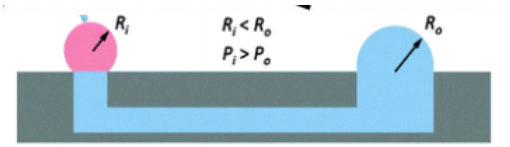

Fig. 1.4. Surface tension pump.[10]

  - **Evaporation pumps**: Based on the different evaporation rates of two different water droplets because of their different size.[11][12]

Fig. 1.5. Evaporation pump.[10]

- **Peristaltic pumps**: Imitate peristalsis by the sequential 'pinching' of actuators which drive the flow in the desired direction depending on parameters such as the actuation frequency. This mechanism requires a source of pressure as well.[13][7]

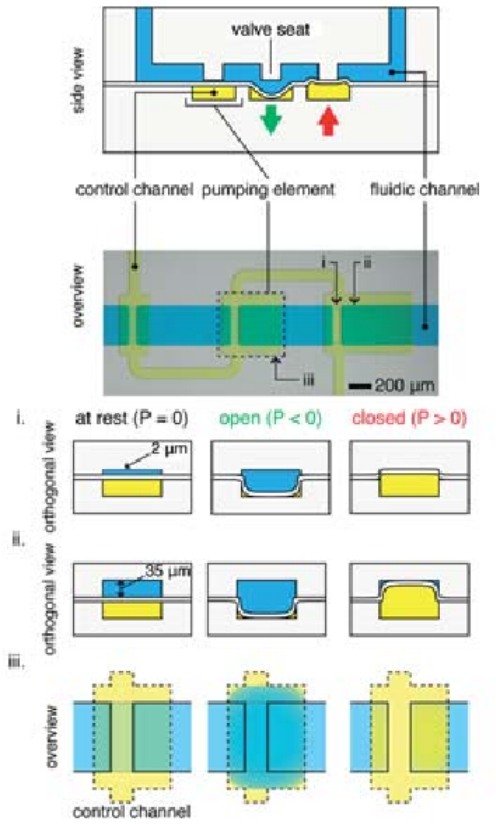

Fig. 1.6. Peristaltic pump.[13]

- **Capillarity pumps**: Based on capillarity forces which could drive a meniscus through a channel or a fluid through a paper sheet.[14][11][15]

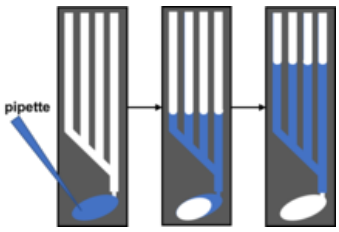

Fig. 1.7. Capillarity pump.

- **Electro-osmotic pumps**: Mechanism that makes use of an electric field to move an uncharged fluid relative to a charged surface. Due to the interaction between the applied electric field and the charged surface, pressure differences which drive the flow are generated.[16][17][18]

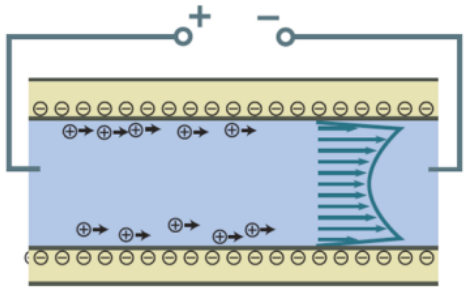

Fig. 1.8. Electro-osmotic pump.

Since the main desired characteristics of control flow mechanisms are ease to use and require low energy consumption, traditional BioMEMS pumping mechanisms focused on syringe pumps, pressure or vacuum driven flows or peristaltic pumps. Later, more portable cheap and disposable solutions arose like capillary flow, gravity-driven flows, surface tension and evaporation-based pumps, etc. However, as these methods do not provide accurate control over the flows or even constant flows, more complex and energy requiring control methods were developed, such as pressure or electrokinetic driven pumps.[16][17][18][19] But since they have also their drawbacks, there is still a need for solutions which satisfy the requirements of allowing a precise control of the flow but without being complex or requiring big amounts of energy.[20][1][2] In particular, this project aims at endowing with better control capabilities one of these techniques.

1.3. PDMS gas solubility as a pumping mechanism

In this project a pumping mechanism is introduced, based on the PDMS affinity for air. The working principle of the pump relies on the dissolution and diffusion of air into a PDMS slab, which generates a negative pressure for driving fluids through microchannels.[1][2] In order for the PDMS to absorb air, it should be previously subjected to a degasification process by being placed in a vacuum chamber for a certain period of time, and later on assembled in a microfluidic system suck the air out of it, which will drag liquid as well.[1][2]

A PDMS pump could be placed at the outlet of a microfluidic channel and generate a pressure-driven flow inside it, but could, at the same time, be the container which would become afterwards filled with the transported fluid.[1] Even bubble absorbance could be another possible application of PDMS gas solubility by the construction of an on-device degasser with a gas-permeable membrane that would retain the non-desired air traps of the microchannels.[1]

But although the PDMS gas solubility property can be used for many different applications in different ways, the main focus of the project will be on the independent modular PDMS pump configuration, represented in figure 1.9.a. A detailed physical description of the pressure-driven flow generated with them will be provided, together with numerical solutions for different geometries that will allow modelling their pumping performance.

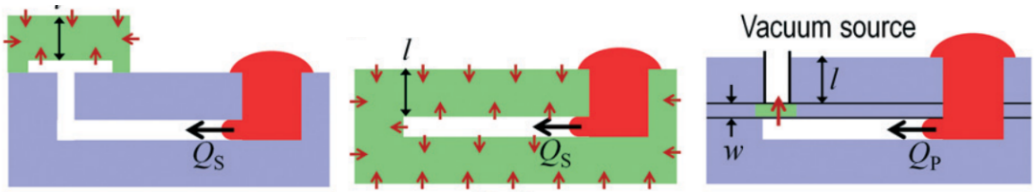

(a) Modular pump at the outlet of a microchannel.[1] (b) Pump acting also as the container.[1] (c) Gas permeable membrane for bubble absorbance.[1]

Fig. 1.9. Possible pumps configurations based on PDMS gas permeability and solubility.

1.3.1. Advantages of degassed PDMS as a pump over other methods

An advantage this new method provides is the fact that **no real-time control over the pumping performance would be needed**, in contrast to other types of pumps such as syringe, pressure based or peristaltic ones.[13] Through the geometry selection of both the PDMS slab and microchannels arrangement, a behaviour would be expected after previous modelling, so depending on the desired flow, a PDMS structure would be built. By varying the geometries of the PDMS slabs or by combining them together, different pumping laws would be obtained.[2] This solves problems of other methods such as electro-osmosis pumps which, apart from being complex and requiring high electric supply, generate flows with extremely small velocities;[18] or, on the contrary, avoid too high fluid speeds that could result in disrupting samples.

In contrast to the bulky or portable but expensive hardware used for electrokinetic pumps,[1][2][17] **simplicity and cheapness** are the main advantages this PDMS pump provides.[1][2] Regardless the integration degree of the pump in the microfluidic system (complete integration or modular behaviour), control over the flow can always be reached through previous modelling and consequently geometry choice. This modelling lies at the heart of this project.

Modular pumps, built independently of the system to be afterwards assembled to it, have the advantage of providing a higher **flexibility in the device design and materials choice**, therefore **reducing their complexity and costs**.[2] Modular

pumps can become attached, removed and replaced to a system and, by varying their geometries, allow changing the pumping performance depending on the application and its requirements.[2] There is no need to transport a pump which usually is several times the size of the device, but instead a sealed bag with a small PDMS slab. Furthermore, depending on the application, modular pumps could become **reusable** by disconnecting them of the system and subjecting them to degasification again; **or disposable** due to their low production cost.

Also, in comparison to methods such as paper-based capillarity pumps or electro-osmotic pumps, **no direct interaction with the fluid** would exist in case of reversible modular pump and, therefore, no surface treatment would be needed and disruption of the sample avoided.[1] One of the main problems of paper capillarity based pumps is clogging. For instance, although it has been achieved, blood is a challenging sample to be driven by paper and previous treatment of the paper is required.[14] Another problem of paper based pumps is that the sample cannot be separated after driven and reused in following steps, the experiment to carry out or sensing mechanism needs to be performed over paper if the sample is driven through it. This problem would not exist if the pump were independent of the fluid, such as modular PDMS pumps. Electro-kinetic driven pumps are also an example of driving flow method which could damage the sample since the direct current that needs to be sustained in electro-osmosis through electrochemical reactions at the electrodes can produce toxic effects and contamination,[21] generate bubbles,[18] hydrodynamic instability[18] or electrode degradation or dissolution.[21]

On the other hand, although this project will be focused on modular pumps that could be assembled to the outlet port of microchannels systems, completely integrated pumps in a PDMS system have also their advantages due to this material's nature.

PDMS is widely used in BioMEMS due to its mechanical, chemical and optical characteristics. Soft lithography is the set of microfabrication techniques used to create devices and generate patterns through micromolded pieces in BioMEMS, and uses mainly PDMS as resin stamp due to its following advantages:[7][1]

- Inexpensive: Between US $ 1 and $ 5 per kilogram.
- Biocompatible: Due to its chemical inertness.
- Easy to fabricate: PDMS in liquid phase becomes cured under heat for a period of time and is easily peeled off from the mould.

- High permeability and solubility to gases: Due to its chemical structure, liquid-like matrix, PDMS allows gas flow and diffusion though it. Property which is strongly dependent on the crosslinking degree.
- Elastic: Flexible PDMS pieces allows some surface patterns and features to change dimensions and makes handling easier.
- Soft: Soft PDMS pieces prevent hard or fragile materials of the system from breaking.
- Optically transparent: Characteristic that allows recording and observation of structures and processes taking place on them.

Although in the integrated pump configuration samples would be in contact with PDMS and surface treatment and control of their solubility over PDMS may be required, as well as autoclaving in case toxic non-crosslinked monomers were present,[7] the gas solubility property of PDMS would not only be used to drive a fluid flow, but also as a **bubble retainer**. This satisfies one of the major needs in BioMEMS microfluidic systems.[1][7]

1.3.2. Parameters that affect the degassed PDMS pumping performance

The effect of several parameters in the PDMS pumping performance has been studied[2] such as the PDMS area in contact with air, PDMS slab volume or the closed system volume. It has also been shown it not only depends on the PDMS geometry but on both the initial volume of air inside the system (including microchannel and PDMS slab) and the crosslinking degree of the PDMS as well.

- **Surface area of the PDMS pump in contact with air**: It has been observed that the driving pressure increases the higher the area in contact with air, steeper the slope of the pressure vs. time curve for higher surface areas. Also, the duration of the pumping activity in equal conditions was observed to decrease for increasing surface areas.[2]
- **PDMS slab volume**: With increased volumes, higher maximum pressures and pumping durations were reached. The effect of this parameter is interesting for applications in which pumping is needed for long times such as cell cultures continuous maintenance.[2]
- **Initial volume of gas containing in the closed system**, outside the PDMS slab: A closed system is a physical system in which mass cannot be transferred in or out. For smaller gas system volumes, higher pumping pressures

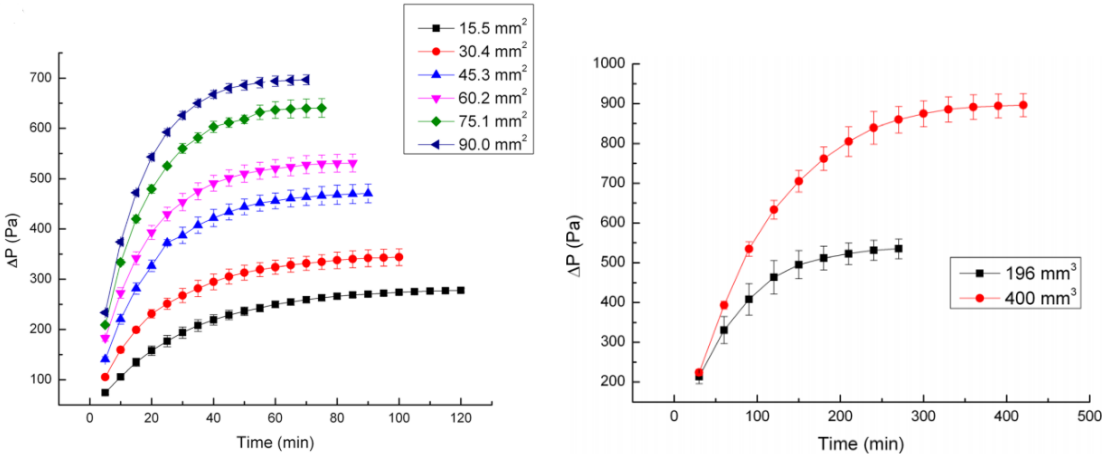

(a) Pressure drop for different areas in contact with air.

(b) Pressure drop for different PDMS slab volumes.

Fig. 1.10. Effect of the area in contact with air and the PDMS slab volume in the pumping performance.[2]

were obtained; being the pumping period directly proportional to the system volumes.[2]

- **Initial volume of air contained in the pump** (PDMS slab): Air contained in the pump at the start of the pumping activity decreases the performance but at the same time could prevent a very abrupt flow start and therefore prevent the system from becoming disrupted.[2]
- **Cross-linking degree of the PDMS pump**: Since the more cross-linker present in the slab, the less actual PDMS volume, and the less pumping pressure is generated.[2]

Once known the parameters that affect the pumping power, through a detailed physical description of the pressure and flow evolutions, numerical solutions for different geometries will be generated. This would allow, in a further step, to precisely design different PDMS slabs as pumps for different applications.

1.3.3. Possible applications of PDMS pumps

Some possible of the several applications of degassed PDMS pumps are:

- **Sample separation due to sedimentation**: In Point-Of-Care (POC) devices sample separation is sometimes an important process that needs to take place for following analysis. Blood is an example of sample that becomes separated through sedimentation. Due to the densities difference between cells and plasma, at certain low flow rates, cells precipitate by gravity. Since PDMS

pumps provide relatively low flow rates, they can be used for samples separation by sedimentation.[1]

- **Cell culture seeding**: Culture seeding in microfluidic channels or devices involves controlling the flows to which cells are subjected since there are some considerations to take into account when carrying out the process. An important step in culture seeding is the cell deposition by either attachment or physical entrapment, and this may not occur for high flow rates; but in very small channels, if the media flow is stopped, depletion of nutrients may happen.[7] Also, the rates of restoring flows or flows itself need to be controlled since cells can become sheared off the substrates or even killed in case a strong pulse were applied or high forces were exerted on the cells.[7][22]

- **Cell culture maintenance**: The low flow rates generated by vacuum-driven pumps are also very suitable for continuously providing with nutrients the cell cultures and its waste products removal. Cells are very sensitive to the microenvironment and concentration gradients are sometimes needed for research as, for instance, tumour 3D modelling.[10] Besides, the fact of being able to transport microfluidics for long periods of time not only allows cells to be continuously supplied with nutrients but to save large amounts of precious reagents due to dealing with fluids at the micro scale.[7][10]

- **Mixing**: For many processes happening in BioMEMS, POC or LOC devices such as DNA and RNA analysis, mercury detection or immunoassays testing, samples need to become mixed for different reactions to occur. By playing with the channels resistance ratios, different flow rates can be achieved and consequent mixture of fluids obtained.[1]

- **Rheological measurements**: For instance, having a reference fluid whose viscosity is known, for equal pumping powers, the viscosity of other fluids could be calculated.[1]

1.4. Regulatory framework

There exist different agencies and companies in charge of ensuring safety and reliability of medical devices, including BioMEMS, and whose approval is compulsory for clinical adoption. In the United States the main agency in charge of regulating medical research is the Food and Drug Administration (FDA), so for a medical device to reach the market, it needs to comply with the FDA regulations; while in Europe it is controlled by the European Medicines Agency (EMA) and the European Conformity (CE) marking, mandatory for some products to be commercially distributed within the European Economic Area (EEA). Furthermore, the World Medical Association defines ethical standards in medical research too.[23] The EMA

ensures safety and that the device performs its claimed functions. However, apart from that, the FDA has additional requirements such as the efficacy one, this means, in the FDA approval process an evaluation is performed regarding if the product currently exists, whether any other complies with the needs the product in question is meant to cover or if there is a real need for it. The FDA therefore is more restrictive than the EMA.[24]

Furthermore, not only mandatory certifications exist, but there are also voluntary standards which ensures quality of products and therefore facilitate their commercial distribution. For instance, the International Organization for Standardization (ISO) is a federation formed by 145 countries that has set the ISO standards, and although adopting them is not compulsory, some countries have been adopted them as part of the regulations needed to approve medical devices.[25] Also, Underwriters Laboratories (UL), a global independent safety science company, provides certification regarding safety and validation and some governmental agencies such as Occupational Safety and Health Administration (OSHA), in charge of ensuring good work conditions, hires it to perform their evaluations.[26]

However, BioMEMS, LOC and POC devices development and clinical adoption takes a long and complicated process. As they are emerging technologies, there is still a lack of regulation and standardization, reason why the approval of many technologies consumes many inefficient efforts. The pathway followed until a device enters the actual clinical world includes a stage termed 'The Valley of Death', where proof of principle and real-world models are required and since the uncovered medical needs are not yet properly understood, and there is still a lack of world-wide collaborations and protocols standards, many of the proposed technologies and devices do not pass the 'Valley of Death'.[27]

2. PHYSICAL MODEL

The mechanism by which the degassed PDMS pump works relies on the absorption of gas into the slab. To do so, the slab needs to be previously degassed by being placed in a vacuum chamber for certain period of time and, afterwards, once placed on a closed fluidic system, it creates a negative pressure for driving fluid through a microfluidic channel.[1][2]

In this chapter the physical description of a closed system consisting of a PDMS slab assembled to a circular crossection channel, containing the fluid to be driven, is provided, as shown in figure 2.1. The PDMS is coated with epoxy resin in all its faces except from the lower one, which is in contact with the air of the microchannel, to maximize the pumping performance.

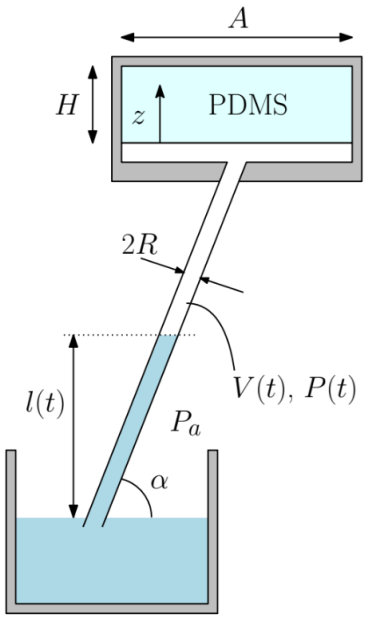

Fig. 2.1. Modular pump at the outlet of a microchannel, depicted here as an inclined pipe that connects the pump with a water reservoir.

2.1. Gas transport in PDMS

The gas absorption of PDMS can be characterized as a solution-diffusion process.[1][2] One of the main advantages of working with PDMS, and, for the case of PDMS pump application the most essential one, is that PDMS is gas soluble and permeable.[1] Although PDMS is a solid, it can be considered as a liquid since its gel-like matrix geometry allows gas transport within it.[1] After placing a PDMS piece in a vacuum desiccator for a certain period, the air within it flows outwards; but when taking it out from the chamber, air is reabsorbed again.

In rubbery polymers, gas solubility depends on the pressure and on the concentration of soluble gases contained in them, and its given by Henry's law.[1][2][28] Thus, as air solution occurs in the wall in contact with PDMS and the molecules

diffuse into the PDMS, Henry's law can be applied, providing the concentration of air at $z = 0$ at any time as

$$C(x, y, 0, t) = K_h P(t); \tag{2.1}$$

where K_h is Henry's constant, $P(t)$ the pressure in the closed system chamber as shown in figure 2.1; while the rest of the surfaces are impermeable as they have been coated with epoxy resin, which means no flux of air is generated through them:

$$\frac{\partial C}{\partial n} = \nabla C \cdot \vec{n} = 0, \tag{2.2}$$

where $\vec{n}$ is the unit vector normal to the surface.

Also, gas transport in PDMS follows Fick's 2^{nd} law of diffusion[1][2][28] which describes the spatio-temporal evolution of the concentration field of the permeated air:

$$\frac{\partial C}{\partial t} = D\nabla^2 C, \tag{2.3}$$

this is,

$$\frac{\partial C}{\partial t} = D\left(\frac{\partial^2 C}{\partial x^2} + \frac{\partial^2 C}{\partial y^2} + \frac{\partial^2 C}{\partial z^2}\right); \tag{2.4}$$

where D denotes the diffusion coefficient of air in PDMS.

Thus, the equations (2.1) and (2.2) represent the boundary conditions of the differential equation that governs the system, equation (2.3). The air diffusion through the PDMS slab follows, therefore, the heat equation with Dirichlet (Henry's law) and Neumann (derivative equal to 0 at the surfaces) boundary conditions.

And being $t = 0$ the moment at which the slab is taken out from the vacuum reservoir and connection with the microchannel occurs, the initial conditions are:

$$C(x, y, z, 0) = 0. \tag{2.5}$$

Note that the molar flux across the PDMS wall in contact with air ($\partial\Omega_1$) is defined as

$$\dot{n} = D\int_{\partial\Omega_1} \nabla C \cdot \vec{n} dS. \tag{2.6}$$

2.2. Motion of a water column through a channel

The water of a microchannel is driven by the negative pressure generated due to the diffusion of air into the PDMS.
The air volume of the microchannel can be expressed as a function of the wetted length $l(t)$ as

$$V(l) = V_0 - \pi R^2 l \tag{2.7}$$

where $V_0 = V(0)$ is the initial volume of air in the microchannel. Thus, the flow rate reads

$$Q(t) \equiv -\dot{V} \equiv \pi R^2 \dot{l} \tag{2.8}$$

The pressure inside the microchannel is the ambient pressure minus the reduced pressure drop due both to hydrodynamic and hydrostatic losses and to the capillary overpressure:[7]

$$P(t) = P_a - \Delta P = P_a - \left[\left(\frac{8\mu}{\pi R^2} Q(l) + \rho g \sin\alpha \right) l + \frac{2\gamma \left| cos\theta \right|}{R} \right] \tag{2.9}$$

where μ is the water dynamic viscosity, ρ its density, α the degree of inclination of the microchannel ($\alpha = 0$ when the channel is horizontal and $\alpha = \frac{\pi}{2}$ when its vertical), γ is the interfacial tension, and θ is the wetting angle of the liquid on the surface of the capillary.

Corresponding to the **hydrodynamic term**, $\frac{8\mu}{\pi R^2} Q(l) l$, comes from the Hagen-Poiseuille equation. This equation describes the pressure drop in a channel where there is an incompressible and Newtonian fluid in laminar flow.[7]

Besides, the **gravity effect** also generates a pressure loss described with the term $\rho g \sin\alpha l$.

And finally, $\frac{2\gamma|\cos\theta|}{R}$ is the **capillary pressure** given by the water-air meniscus. Capillary pressure is the pressure difference between two immiscible fluids in a tube, resulting from the interactions of forces between the fluid and solid walls of the channel.[7]

Note that ΔP can be written in terms of R_h, the hydraulic resistance, as

$$\Delta P = P_a - P(t) = R_h(l) Q(l) + \rho g \sin\alpha l + \frac{2\gamma \left| \cos\theta \right|}{R} \tag{2.10}$$

where the pressure term $R_h(l)Q(l)$ is the pressure needed to overcome to transport through a given network with resistance R_h the flow Q. This notation will allow in a future to substitute the term R_h for the corresponding resistance of the given microfluidic system.[7] Depending on the microfluidic system configuration, this hydraulic resistance could be computed in an analogue way to electric circuits for relatively simple geometries or by experimental characterization for more complex ones.[7]

2.3. Coupling the PDMS diffusion and the microfluidic flow problems: Pressure-driven flow

The ideal gas law couples the gas transport in PDMS with the motion of the fluid in the microchannel by relating the volume $V(t)$ and pressure $P(t)$ of the microchannel with the number of air moles $n(t)$ contained:

$$PV = nR_uT, \tag{2.11}$$

where R_u is the gas constant and T the temperature of the system. After taking it's time derivative,

$$\dot{P}V + P\dot{V} = \dot{n}R_uT, \tag{2.12}$$

both the pressure and the air concentration terms can become related. Once having the pressure P and the volume V in terms of the wetted length $l(t)$ and the molar flux $\dot{n}$ in terms of the concentration field C, by introducing them in equation (2.12), both the air diffusion into PDMS and water flow through the microchannel become related by a 2^{nd} order Ordinary Differential Equation (ODE). To do so, the equations have been written in dimensionless form first.
τ is the dimensionless time,

$$\tau = \frac{D}{H^2}t,$$

and the dimensionless pressure drop $\tilde{P}(\tau)$, wetted length $\eta(\tau)$ and mole number $\phi(\tau)$ read

$$\tilde{P} = 1 - \frac{P}{P_a} = \frac{\Delta P}{P_a},\ \eta = \frac{\pi R^2 l}{V_0} = 1 - \frac{V}{V_0},\ \phi = \frac{R_uT}{P_aV_0}n. \tag{2.13}$$

Thus, if defining the characteristic time, length and flow rate as

$$t_c = \frac{H^2}{D},\ l_c = \frac{V_0}{\pi R^2},\ Q_c = \frac{V_0 D}{H^2},$$

and the dimensional time, length, flow rate and pressure can be easily obtained from the dimensionless ones:

$$t = t_c\tau,\ l = l_c\eta, Q = Q_c\eta',\ \Delta P = P_a\tilde{P}(\eta).$$

The dimensionless pressure variation can, therefore, be written as

$$\tilde{P}(\eta) = \left(\frac{8\mu l_c^2 D}{P_a H^2}\eta' + \frac{\rho g l_c \sin\alpha}{P_a}\right)\eta + \frac{2\gamma\left|\cos\theta\right|}{RP_a} = \left(\Omega_d\eta' + \Omega_h\right)\eta + \Omega_c \tag{2.14}$$

where Ω_d, Ω_h and Ω_c are the dimensionless constants hydrodynamic resistance, the hydrostatic one and the capillary resistance respectively.

The dimensionless molar flux ϕ' reads

$$\phi' = -\beta\int_{\partial\tilde{\Omega}_1}\tilde{\nabla}\tilde{C}\cdot\vec{n}d\tilde{S}, \tag{2.15}$$

where $\tilde{\nabla}$, $d\tilde{S}$ and $\partial\tilde{\Omega}_1$ are the dimensionless ∇, dS and $\partial\Omega_1$, and $\beta = (K_h R_u T)(AH/V_0)$, the product of solubility and PDMS-to-air volume ratio.

Finally, introducing the dimensionless pressure, volume and molar flux in equation (2.12), the following relation is obtained

$$\Omega_d(1-\eta)\eta\eta'' + \left[\left(\Omega_d\eta' + \Omega_h\right)(1-2\eta) + 1 - \Omega_c\right]\eta' = -\phi', \tag{2.16}$$

the 2^{nd} order Ordinary Differential Equation (ODE) which relates the air diffusion in PDMS with the water flow through the microchannel. Note that the order of magnitude of the dimensionless constant Ω_d is $O(10^{-11})$ (see table 6.2 with values), much smaller than the rest of the constants, making the terms multiplied by it neglectable and becoming an approximation to the solution:

$$\left[\Omega_h(1-2\eta) + 1 - \Omega_c\right]\eta' = -\phi', \tag{2.17}$$

where the initial conditions for η and η' are

$$\eta(0) = 0,\ \eta'(0) = \frac{-\phi'(0)}{1 + \Omega_h - \Omega_c}. \tag{2.18}$$

2.4. Solution to the problem in 1D

2.4.1. Analytical solution

By the method of separation of variables, the solution of the concentration that satisfies the problem (2.1) - (2.5) reads

$$\frac{C(z,t)}{K_h P_a} = 1 - \frac{2}{\pi}\sum_{n=0}^{\infty}\frac{1}{n+1/2}\exp\left\{-\pi^2\left(n+\frac{1}{2}\right)^2\frac{Dt}{H^2}\right\}\sin\left\{\pi\left(n+\frac{1}{2}\right)\frac{z}{H}\right\}; \tag{2.19}$$

and the diffusive molar flow rate absorbed by PDMS (equation (2.6)) is

$$-\dot{n} = -AD\frac{\partial C}{\partial z}(0,t) = \frac{2ADK_hP_a}{H}\sum_{n=0}^{\infty}\exp\left\{-\pi^2\left(n+\frac{1}{2}\right)^2\frac{Dt}{H^2}\right\}. \tag{2.20}$$

Being, thereby, the solution to the dimensionless molar flow rate

$$-\phi' = 2\beta\sum_{n=0}^{\infty}\exp\left\{-\pi^2\left(n+\frac{1}{2}\right)^2\tau\right\}. \tag{2.21}$$

2.4.2. Finite Differences

An implementation to solve the 1D problem was also made in a Matlab script using the Finite Differences method and the suite of ODE solvers Matlab provides. Integrals were performed to obtain a numerical solution of both the concentration field of the spatial domain along time and the length of the column of water (wetted

length) and its derivative.

The integrator used has been ode23, an implementation of an implicit Runge-Kutta method.[29] ode23 is a three-stage, third-order method. It is faster than the ode45 that implements a Runge-Kutta method of fourth order with adaptive time step.[30]

To solve the problem, the system (2.1) - (2.5), which defines the gas transport in PDMS, has been defined in a dimensionless form with

$$\tilde{C} = \frac{C}{K_h P_a},\ \xi = \frac{z}{H},\ \tau = \frac{D}{H^2}t.$$

Dimensionless equation (2.4) in 1D reads

$$\frac{\partial \tilde{C}}{\partial \tau} = \frac{\partial^2 \tilde{C}}{\partial \xi^2}; \tag{2.22}$$

and the boundary conditions and initial conditions

$$\tilde{C}(0,\tau) = \frac{K_h P(t)}{K_h P_a} = 1 - \tilde{P}, \tag{2.23}$$

$$\frac{\partial \tilde{C}}{\partial \tau}(1,\tau) = 0, \tag{2.24}$$

$$\frac{\partial \tilde{C}}{\partial \tau}(\xi,0) = 0. \tag{2.25}$$

By using the Finite Differences method, a spatial discretization is made over the domain as shown in figure 2.2 and the PDE and the boundary conditions are converted into a system of ODEs that can be integrated using the integrator Matlab provides.[30]

The one dimensional spatial domain is discretized in a uniformly spaced grid of $N = 100$ points, ξ_i, such that

$$\xi_i = (i-1)\Delta\xi \ for\ i = \{1, ..., N\} \tag{2.26}$$

where $\Delta\xi = 1/(N-1)$, corresponding $\xi = 0$ to $i = 1$ and $\xi = 1$ to $i = N$.

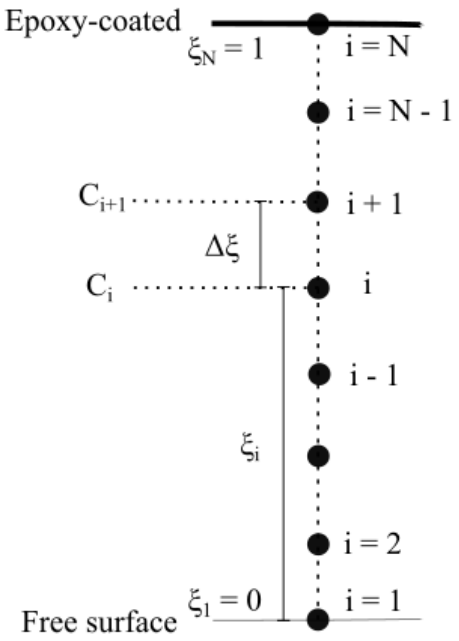

Fig. 2.2. Spatial discretization. Domain divided by N nodes in $N-1$ pieces of length $\Delta\xi$.

Therefore, since the PDE (2.22) is fulfilled at every node, it yields to the following set of ODEs

$$\frac{\partial \tilde{C}_i}{\partial \tau} = (\frac{\partial^2 \tilde{C}}{\partial \xi^2})_{\xi=\xi_i} \; for \; i = \{1, ..., N\}\,, \tag{2.27}$$

and after substituting the derivatives to their finite difference approximation, it can be rewritten as:

$$\frac{\partial \tilde{C}_i}{\partial \tau} = \frac{\tilde{C}_{i+1} - 2\tilde{C}_i + \tilde{C}_{i-1}}{(\Delta\xi)^2} \; for \; i = \{2, ..., N-1\}\,. \tag{2.28}$$

Notice that at nodes $i = 1$ and $i = N$ this expression is not satisfied, but the concentration at those nodes is defined by the boundary conditions.
At $i = 1$, from 2.23, the surface in contact with air is

$$\tilde{C}_1 = 1 - \tilde{P}, \tag{2.29}$$

and at $i = N$, the dead end with no mass flux,

$$\tilde{C}_N = \frac{4\tilde{C}_{N-1} - \tilde{C}_{N-2}}{3}. \tag{2.30}$$

The integrator obtains a solution for the concentration field (concentration at each node) and the wetted length and its derivative at each time step. It does so by integrating the left side of equation (2.28), with the right side given by the finite differences at each node; and obtains η and η' by integrating η' and η'' respectively.

η'' is obtained from ϕ', η and η' as expressed in equation (2.16); and ϕ' is calculated through finite differences from the concentration field as

$$\phi' = \beta \left(\frac{-3\tilde{C}_1 + 4\tilde{C}_2 - \tilde{C}_3}{2\Delta\xi} \right), \tag{2.31}$$

which represents the dimensionless molar flux (2.15).

To sum up, at each time step the derivatives of the concentration are obtained by their finite differences, and are integrated together with the derivatives of the length and length derivative by ode23s, obtaining finally a matrix which contains the values of the concentration at each node, the length of the water column and its derivative at each time step.

2.5. Contribution of a narrowing (needle) to the pressure drop

The actual model used for experiments consisted on a test tube with its tip filled with PDMS, connected to a microchannel through a needle. The needle was connecting the microfluidic channel and the air buffer in contact with the PDMS surface.

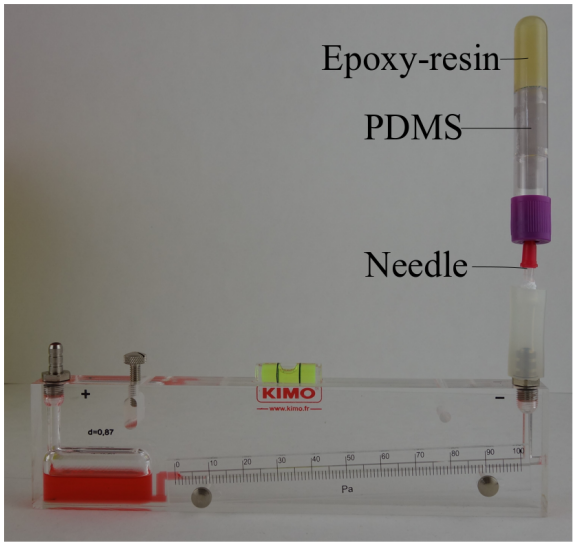

Fig. 2.3. Experiments setup in which a PDMS containing test tube is connected to pipe attached to a liquid reservoir through a needle. Provided by Yara Álvarez, from UPV microfluidics research team.

Therefore, another consideration to take into account that could affect in the physical description of the problem in order to compare theoretical and experimental results was an extra pressure drop **hydrodynamic term**[7] given by the flow of air through that needle. It existed the doubt that given the small diameter of the needle, it could significantly contribute to the pressure loss that the pump must overcome.

Considering the system PDMS - chamber of air - needle - microchannel - fluid

shown in figure 2.3, there is another pressure drop from the pressure of the chamber of air in contact with PDMS and the pressure in the microchannel, apart from the drop already evaluated from the channel pressure to the atmospheric one.

If taking into account that extra pressure drop, the dimensionless hydrodynamic pressure drop is written as:

$$\tilde{P}_{hydrod}(\eta) = \Omega_d \left(\eta + \frac{\mu_{air}}{\mu} \frac{R^2}{R^2_{needle}} \frac{l_{needle}}{l_c} \right) \eta' \tag{2.32}$$

Notice that the pressure term given by the needle is equivalent to having a longer channel,

$$l_{eq} \approx \frac{\mu_{air}}{\mu} \frac{R^2}{R^2_{needle}} l_{needle}.$$

From parameters in table 6.2, l_{eq} is $5.76mm$.

So, in order to evaluate the effect of the needle in the system, from

$$\tilde{P}_{hydrod}(\eta) = \Omega_d \left(\eta + \frac{l_{eq}}{l_c} \right) \eta', \tag{2.33}$$

where the term $\Omega_d \frac{l_{eq}}{l_c}$ has an order of magnitude of $O(10^{-13})$, even smaller than the order of magnitude of the hydrodynamic resistance Ω_d itself, $O(10^{-11})$, it can be concluded that the pressure term given by the needle can also be neglected. For the needle contribution to the pressure drop to be the same order as the water hydrodynamic term,

$$\frac{l_{eq}}{l_c} \approx 1,$$

and a needle of around $1m$ length is needed.

2.6. Extension of the model to more complex geometries

2.6.1. Definition of the gas diffusion problem in cylindrical coordinates

Solving the PDMS diffusion problem in 2D cylindrical coordinates provides a 3D solution corresponding to a cylindrical PDMS slab. This is why the problem is being defined also in cylindrical coordinates, because some of the simulations carried out in the project have been done this way.

Being r the distance to the axis and z the distance along the axis, the system (2.1) - (2.5) is expressed cylindrical coordinates, where the concentration field depends on r, z and time t, $C(r, z, t)$.

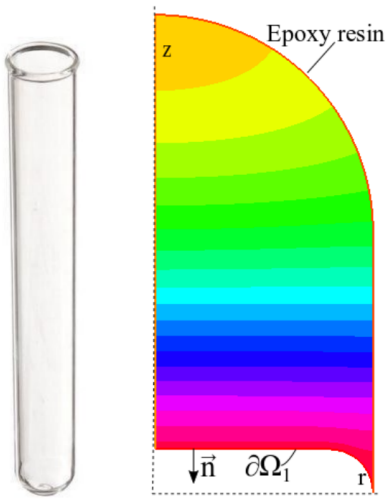

Fig. 2.4. Test tube simulation with FreeFem++. The radius of the test tube is of 5mm.

The diffussion equation reads

$$\frac{\partial C}{\partial t} = D\left(\frac{1}{r}\frac{\partial}{\partial r}\left(r\frac{\partial C}{\partial r}\right) + \frac{\partial^2 C}{\partial z^2}\right), \tag{2.34}$$

with boundary condition at $z = 0$, the PDMS wall in contact with air,

$$C(r, 0, t) = K_h P(t), \tag{2.35}$$

and boundary condition at the rest of the impermeable walls, where there is no air flux,

$$\frac{\partial C}{\partial n} = 0, \tag{2.36}$$

and initial conditions of

$$C(r, z, 0) = 0. \tag{2.37}$$

The molar flux through the free wall ($\partial\Omega_1$), (2.6), is written

$$\dot{n} = D\int_{\partial\Omega_1} 2\pi r \nabla C \cdot \vec{n} dS. \tag{2.38}$$

Note that the term $2\pi r$ is the curvature factor which appears when defining the molar flux through a wall.

2.6.2. Empty interior in the PDMS slab

A new design of the PDMS structure was proposed and modeled, a PDMS block with an empty hole in its interior, as shown in the figure 2.5.

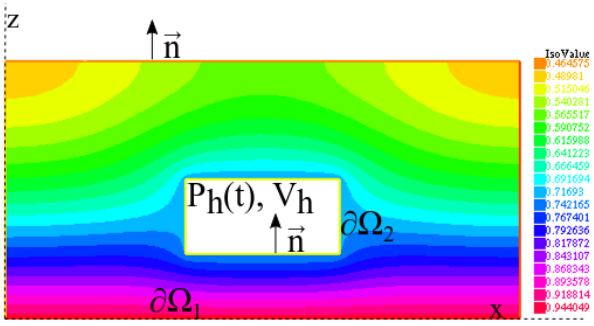

Fig. 2.5. PDMS slab with an empty hole in its interior. The length of the slab is 1cm and the height 5mm.

In order to model with the FEM this new structure, the pressure inside the hole of the PDMS should be also modeled and taken into account, being the boundary condition at the walls of the hole the Henry's law as well.

Being P_h the pressure in the hole, V_h the volume of the hole and n_h the air moles inside it, after taking the time derivative at both sides of $P_h V_h = n_h R_u T$

$$\dot{P}_h V_h = \dot{n}_h R_u T \tag{2.39}$$

is obtained as the volume inside the hole is constant, where

$$\dot{n}_h = -D \int_{\partial\Omega_2} \nabla C \cdot \vec{n} dS, \tag{2.40}$$

and $\partial\Omega_2$ the area of PDMS in contact with the hole.

Therefore, from (2.40) and (2.39), the pressure inside the hole reads

$$\dot{P}_h = \frac{R_u T}{V_h} \left(-D \int_{\partial\Omega_2} \nabla C \cdot \vec{n} dS \right). \tag{2.41}$$

Finally, through the dimensionless concentration and pressure in the hole

$$\tilde{C} = \frac{C}{K_h P_a}, \; \tilde{P}_h = \frac{P_h}{P_a} \tag{2.42}$$

equation (2.41) can be written in dimensionless form as

$$\tilde{P}'_h = \left(\frac{V_0}{V_h} \right) \left(\frac{H l_c}{A} \right) \phi'_h \tag{2.43}$$

where ϕ'_h, the dimensionless molar flux inside the hole, is

$$\phi'_h = -\beta \int_{\partial\Omega_2} \tilde{\nabla} \tilde{C} \cdot \vec{n} d\tilde{S}. \tag{2.44}$$

3. SIMULATIONS WITH THE FINITE ELEMENT METHOD

3.1. Introduction to Finite Element Method

3.1.1. Definition and applications

The finite element method or FEM is a general numerical method to discretize a differential equation over a domain to obtain approximate solutions of continuum problems. Due to the difficulty or impossibility of obtaining analytical solutions to these problems, the FEM is a very good approach to the solution for practical purposes.[31][32][33][34]

The FEM handles in a very natural way unstructured meshes which allows dealing with complex geometries and, thereby, to perform computations over different spatial domains in engineering or physics fields.[31] FEM has been chosen to solve the PDMS diffusion problem, with no doubt, due to this feature. It is the only existing method that allows to deal with such freedom different geometries.

It can provide solutions in mass transport, fluid flow, structural analysis, heat transfer or electromagnetic potential problems; or even enable the creation of complex physical or biological systems simulations. It is a tool for developing and improving the design of products, which grants it many industrial applications.[31]

3.1.2. Summary of the method

The method consists in dividing the whole problem into smaller and simpler parts denominated **finite elements** to be afterwards assembled again. Not only the domain is submitted to a partition procedure into subdomains (finite elements), but also, the problem formulation is projected over those subdomains through a set of functions called **base** or **shape functions**. Each finite element is modeled by simple equations with matching properties at the vertices and edges of the finite elements. This allows them to be assembled together and, therefore, yield a solvable system of equations that governs the whole problem for the entire domain. The system of equations is collected in the so called **Stiffness matrix** and the unknowns represent the solution of the problem over each node; the solution over the whole domain is then obtained by interpolating the unknowns values through the base functions.[31]

3.1.3. Elements order and base functions choice

The **finite elements** can be defined as the result of discretizing a given domain. Each finite element is built by the union of different representative points named nodes. Two nodes are adjacent if they belong to the same finite element and a node in the border of a finite element can belong to two finite elements.[31] The resulting ensemble of nodes (and therefore finite elements) is called mesh. Each finite element must fulfill:[35]

1. $\Omega = \cup_n^{e=1} \Omega^{(e)}$.
2. Each $\Omega^{(e)}$ is a compact domain with a continuous boundary.
3. int $(\Omega^{(i)}) \cap$ int $(\Omega^{(j)}) = 0$ for $i \neq j$.

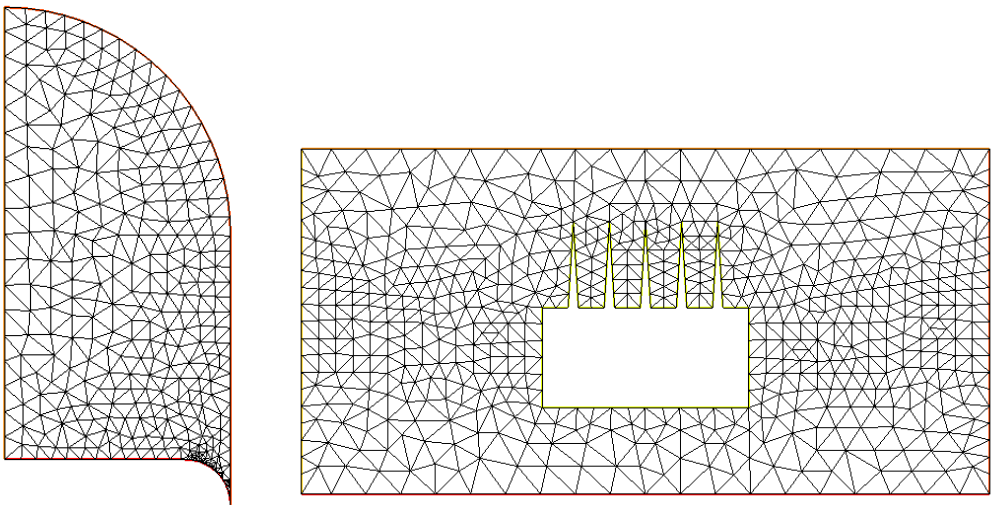

Fig. 3.1. Meshes generated with FreeFem++.

The **finite element space** is a set of functions which work as a base for the projection of the problem over each element. It is a finite-dimension function space V_h, subspace of the Hilbert space H. These **base functions** that form the space are functions of x in 1D, x and y in 2D and x, y and z in 3D and their linear combinations are termed shape functions.[36]

The solution to the problem can be then expressed as a linear combination of those base functions. Over each element, a function space is defined and functions on the finite elements have matching properties at the vertices and edges. This

means, over each node a group of relations between unknown variables is yield. By assembling the relations given on each node for the entire domain, a system of algebraic equations is obtained. These relations, therefore, follow a connectivity or positioning criteria. The resulting equations are the components of the so called **Stiffness matrix**, which unknowns represent the approximate values to the solution in specific discrete points of the domain. Being, thereby, the final number of equations proportional to the number of nodes.[34][35] The system of equations is finally solved by the fastest mathematical methods to solve systems such as the Gaussian elimination algorithm.[31]

In the following images an example of Bessel function interpolation 1D can be observed.

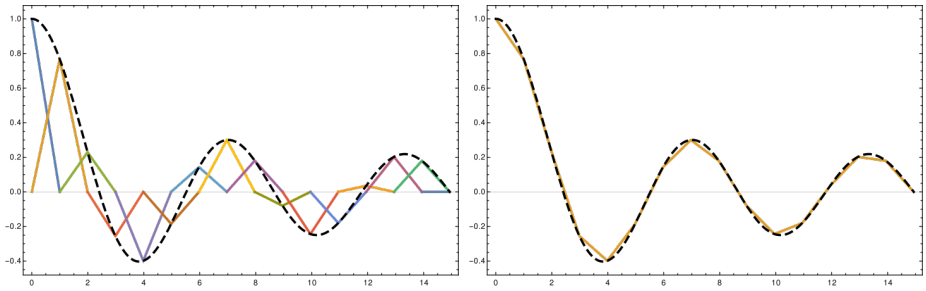

(a) Scaled linear basis functions (shape functions).

(b) Combination of basis functions for reproduce the solution.

Fig. 3.2. 1D Bessel function interpolation through FEM.[35]

The unknowns defined over each node are also denoted by **degrees of freedom**[31] and depend on the type of analysis to perform. For instance, in structural analysis there are three degrees of freedom, the displacements on x, y and z directions; while in thermal analysis a unique unknown exists for each node, the temperature. As the diffusion problem follows the heat equation but instead dealing with temperature, the unknown is the concentration, the number of nodes is the number of degrees of freedom (one unknown per node) and coincides with the dimensions of the finite element space.

The finite **element order** choice is given by the degrees of freedom of the system. In first order elements the base functions used to project the problem are linear, in second order elements they are quadratic and so on. Therefore, to solve the PDMS diffusion problem, linear base functions (first order elements) have been chosen as there is only one unknown defined over each node (one degree of freedom).[34]

Depending on the type of domain, different finite element structures can be

taken, for instance, for first order elements, in 2D domains, triangles o rectangles could be chosen. The following image shows squared 2D linear and quadratic base functions respectively in a squared mesh:

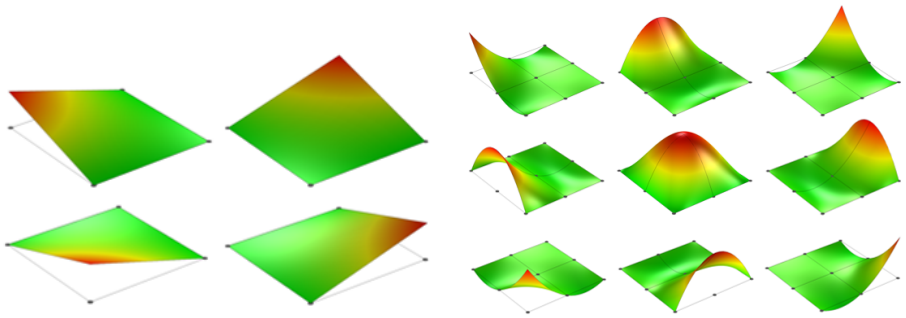

(a) 2D linear base functions. (b) 2D quadratic base functions.

Fig. 3.3. Squared 2D base functions.[34]

Whereas this one is an example of linear base functions in a triangular meshed 2D domain, the one chosen for the approximation of the diffusion problem in FreeFem++:

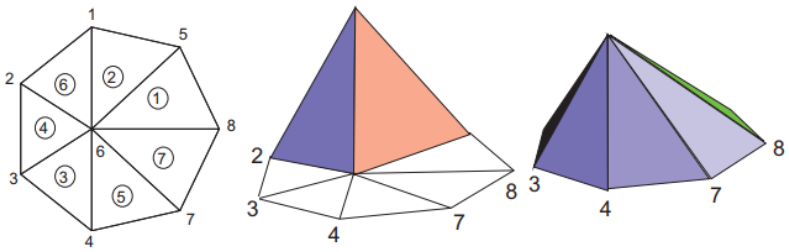

Fig. 3.4. Triangular 2D linear base functions.[36]

It can be observed that each shape function has a value of 1 at a node and 0 at the rest, thereby becoming each finite element defined by linear combinations of different base functions.

The base functions contribute to the system of equations collected in the stiffness matrix when they overlap, but it is 0 when they do not overlap. They diagonal of the stiffness matrix is formed by combinations of base functions which overlap. Both situations are represented in the following figures:

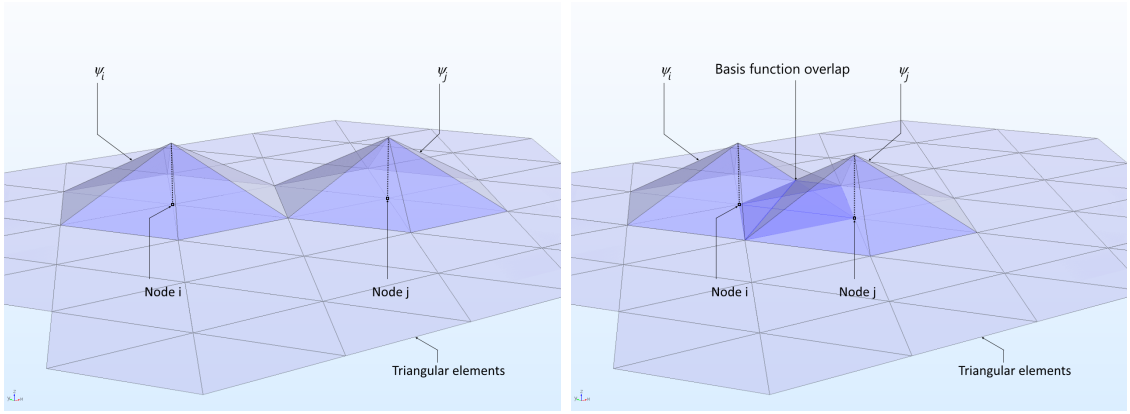

(a) Base functions do not overlap.

(b) Base functions overlap.

Fig. 3.5. 2D base functions.[34]

3.1.4. FEM Features

FEM is a very applicable method in general and its error can be computed under reasonable costs.

The most remarkable feature this procedure has, as previously stated, is its ability of modeling very complex, arbitrary or even time-varying geometries of non-homogeneous problems that other methods cannot handle. It does so by the aforementioned partition process over the whole problem and its domain. FEM allows to interpolate the solution of a problem in a smoothly way for a given structure.[31]

Hence, the main benefit of the method is the flexibility of geometry selection and handling. The fact of subdividing the domain allows to deal with unstructured meshes and, therefore, compute the solution in a more efficient way, concentrating more nodes where the solution changes abruptly and more precision is needed.[34]

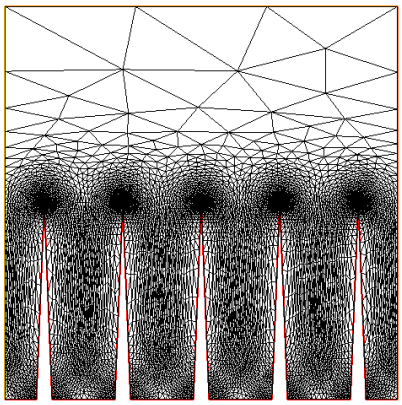

Fig. 3.6. Unstructured mesh in FreeFem++. Notice the fine resolution close to the tips of the wells, where fast variations of the solution are expected.

Besides, apart from the elements size and time step, the accuracy of the solution depends on the choice of the base functions. This could be considered as an advantage as there is even more "control" over the solution obtained.[34]

But on the other hand, a drawback this method has (like every methods) is that it requires many nodes in sharp geometries as edges, as the ones in the peaks of some of the modeled structures in this project. However, this is handled in FEM better than with other methods since FEM allows to place nodes only when they are needed.

3.2. Theoretical foundations

3.2.1. Weak formulation

In order to be able to apply this method, the differential equations need to be written in weak formulation. Weak formulation is also termed *variational* formulation, name with origin in the calculus of variations (small changes in functions).[37] This can be done once the equations that describe the diffusion problem are defined with their corresponding boundary conditions and the normal vector identified (pointing outwards of the surface in this case).

Weak formulation of a differential equation problem is an alternative way of writing those equations in integral form. It is a powerful tool because the equation to solve is not required to be fulfilled at all points of the domain and provides weak solutions only with respect to certain **test functions** v. By weak solutions its meant that the restrictions about continuity of the function and its derivatives become relaxed.[37][34]

In particular, the heat equation that describes the diffusion problem of air into PDMS is

$$\frac{du}{dt} = \nabla^2 u. \tag{3.1}$$

Notice that to adapt the notation to that customarily used in FEMs, $u(x, y, z, t)$ the dimensionless concentration field $\tilde{C}$.

After multiplying 3.1 by a test function v and integrating over the domain Ω at both sides of the equation and introducing Green's first identity $\nabla \cdot (v\, \nabla u) = \nabla v \cdot \nabla u + v\nabla^2 u$, it becomes

$$\int_\Omega (v\frac{du}{dt} + \nabla u \cdot \nabla v)\, dV - \int_\Omega \nabla \cdot (v\, \nabla u)\, dV = 0, \tag{3.2}$$

where the second integral, through the Gauss Divergence Theorem[38] is

$$\int_\Omega \nabla \cdot (v\, \nabla u)\; dV = \int_{\partial\Omega} v\, \nabla u \cdot \vec{n}\, dS. \tag{3.3}$$

Since $\frac{\partial u}{\partial n} = \nabla u \cdot \vec{n} = 0$ (as there is no air loss from the PDMS walls, except the one where the Henry's condition is imposed) and $\frac{du}{dt} = \frac{u-u_0}{\Delta t}$ (where u_0 is the initial concentration), equation 3.2 can be rewritten as

$$\int_\Omega v \left(\frac{u-u_0}{\Delta t}\right)\; dV + \int_\Omega (\nabla u \cdot \nabla v)\, dV = 0, \tag{3.4}$$

which represents the weak formulation of the diffusion problem 3.1, and is written in 2D

$$\int_{\partial\Omega} v \left(\frac{u-u_0}{\Delta t}\right)\; dS + \int_{\partial\Omega} \left(\frac{du}{dx}\frac{dv}{dx} + \frac{du}{dy}\frac{dv}{dy}\right)\; dS = 0. \tag{3.5}$$

In cylindrical coordinates, being the concentration field a function of the radius and the height of the cylindrical domain, $u(x, r, t)$, the weak formulation of the problem reads

$$\int_\Omega rv \left(\frac{u-u_0}{\Delta t}\right)\; dV + \int_\Omega r(\nabla u \cdot \nabla v)\, dV = 0, \tag{3.6}$$

which in 2D is expressed as

$$\int_{\partial\Omega} rv \left(\frac{u-u_0}{\Delta t}\right)\; dS + \int_{\partial\Omega} r\left(\frac{du}{dr}\frac{dv}{dr} + \frac{du}{dz}\frac{dv}{dz}\right)\; dS = 0. \tag{3.7}$$

By removing the Laplacian, the equation needs to be fulfilled for every test function v in the test function space instead of being fulfilled for every point of the domain Ω; and thereby, there is no need for the 2^{nd} derivative to exist in all points, the equality of the equation is required only in an integral sense.[37][34][31] Although this feature of the method is not strictly needed to solve this problem since the concentration function is continuous in all the points of the domain, stating the problem this way demands less from the test functions.

Both the solution u and the test function v belong to a Hilbert subspace, infinite-dimensional function set V;[34] although this function space is approximated to a finite system of algebraic equations (finite dimensional space V_h). Actually, after applying the finite element method over these functions, they become ordinary vectors (i.e. consisting of a finite number of real numbers).[34]

3.2.2. Discretization and variational problem projection

An example of the diffusion problem interpolation in 1D can be developed for further understanding:

The concentration field $u(x)$ along the domain can be expressed as an approximation u_h ($u \approx u_h$) through a linear combination of base functions ψ_i.

$$u_h(x) = \sum_i C_i \psi_i(x) \tag{3.8}$$

In 1 dimension, being L_e the length of the domain, equation 3.4 can be rewritten as

$$\int_0^{L_e} v \left(\frac{u - u_0}{\Delta t} \right) dx = \int_0^{L_e} \frac{du}{dx} \frac{dv}{dx} dx. \tag{3.9}$$

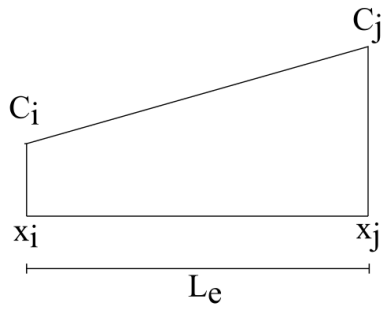

Fig. 3.7. Finite element situated between x_i and x_j where the concentrations are C_i and C_j.

Consider a unique finite element with nodes i and j situated at x_i and x_j respectively. As the polynomial interpolation of 1^{st} order is $u(x) = a + bx$, for the finite element, equations

$$\begin{cases} C_i = a + bx_i \\ C_j = a + bx_j \end{cases} \tag{3.10}$$

are fulfilled over the element nodes, being C_i and C_j the unknown concentrations at nodes i and j.

As the distance between nodes is known, $L_e = x_j - x_i$, from 3.10 the concentration $u(x)$ could be interpolated between any point x_j and x_i as

$$u(x) = C_i \left(\frac{x_j - x}{L_e} \right) + C_j \left(\frac{x - x_i}{L_e} \right) \tag{3.11}$$

where $S_i = -\left(\frac{x_j - x}{L_e}\right)$ and $S_j = \left(\frac{x - x_i}{L_e}\right)$ are the shape functions, linear combinations of the base functions.

Being

$$\vec{N}(x) = (-S_i \;\; S_j) \tag{3.12}$$

and

$$\vec{c} = \begin{pmatrix} C_i \\ C_j \end{pmatrix} \tag{3.13}$$

the vector of unknowns, $u(x)$ can also be written as

$$u(x) = \vec{N}(x)\ \vec{c}\ . \tag{3.14}$$

and $v(x)$, the test or weight function, as

$$v(x) = \vec{c^T}\vec{N^T}(x). \tag{3.15}$$

Note that in this case the test functions are the same as the base functions, proper of the Galerkin method. A Galerkin method, in numerical analysis, is the one by which a continuous operator problem is converted into a discrete one. By doing this selection, the FEM formulated can be considered as a Galerkin method. Nevertheless, not all finite element methods do that; and yet, even for the Galerkin method or for any other, there are plenty of ways of choosing the base functions.[31][34]

Then, by introducing 3.14 and 3.15 in equation 3.9, the following expression is obtained

$$\int_{x_i}^{x_j} \frac{d\ \vec{N^T}}{dx}\frac{d\ \vec{N}}{dx}dx\ \vec{c}\ \ = \int_{x_i}^{x_j}\ \vec{N^T}\left(\frac{\vec{N}(x)\ \vec{c}\ -\ u_0}{\Delta t}\right)dx \tag{3.16}$$

and after doing some algebra,

$$\int_{x_i}^{x_j}\left(\frac{d\ \vec{N^T}}{dx}\frac{d\ \vec{N}}{dx} - \frac{1}{\Delta t}\ \vec{N^T}\vec{N}\right)dx\ \vec{c}\ \ =\ \ -\frac{1}{\Delta t}\int_{x_i}^{x_j}\ \vec{N^T}\ u_0\ \ dx, \tag{3.17}$$

were $\vec{c}$, the vector of unknowns, has become isolated.

3.2.3. System of algebraic equations

Since the element length is L_e, after introducing $\frac{d\vec{N}}{dx} = \left(-\frac{1}{L_e}\ \ \frac{1}{L_e}\right)$ in 3.17 and integrating between 0 and L_e (the element length), 3.17 can be written as

$$k\ \vec{c}\ \ = f. \tag{3.18}$$

where $\vec{c}$ is the vector of unknowns and k, the stiffness matrix such that

$$k = \begin{pmatrix} k_{ae} & k_{be} \\ k_{ce} & k_{de} \end{pmatrix}, f = \begin{pmatrix} f_{ae} \\ f_{be} \end{pmatrix} \tag{3.19}$$

where

$$k_{ae} = \frac{1}{\Delta t}\left(-\frac{L_e}{3} + x_j + \frac{x_j^2 + \Delta t}{L_e}\right), \tag{3.20}$$

$$k_{be} = \frac{1}{\Delta t}\left(-\frac{L_e}{3} + \frac{x_i + x_j}{2} - \frac{x_i x_j + \Delta t}{L_e}\right), \tag{3.21}$$

$$k_{ce} = \frac{1}{\Delta t}\left(\frac{L_e}{3} + \frac{x_i + x_j}{2} + \frac{x_i x_j - \Delta t}{L_e}\right), \tag{3.22}$$

$$k_{de} = \frac{1}{\Delta t}\left(-\frac{L_e}{3} + x_i + \frac{x_i^2 + \Delta t}{L_e}\right), \tag{3.23}$$

$$f_{ae} = \frac{u_0}{\Delta t}\left(\frac{L_e}{2} - x_j\right), \tag{3.24}$$

$$f_{be} = \frac{u_0}{\Delta t}\left(-\frac{L_e}{2} + x_i\right). \tag{3.25}$$

Equation 3.18 represents the final system of equations obtained to solve the problem over a finite element e of length L_e delimited by nodes i and j in 1D.

Therefore, the global stiffness matrix for a domain divided in N elements is obtained by assembling the relations given on each finite element, since they have matching properties at the edges and vertices. The global stiffness matrix is

$$K\vec{C} = F, \tag{3.26}$$

such that

$$K = \sum_{e=1}^{N} k^{(e)}, F = \sum_{e=1}^{N} f^{(e)} \tag{3.27}$$

where the subindex e denotes the element number.

For instance, for a system of three elements, the final system of equations would be expressed as:

$$\begin{pmatrix} k_{a1} & k_{b1} & 0 & 0 \\ k_{c1} & k_{d1} + k_{a2} & k_{b2} & 0 \\ 0 & k_{c2} & k_{b2} + k_{a3} & k_{b3} \\ 0 & 0 & k_{c3} & k_{d3} \end{pmatrix} \begin{pmatrix} C_i \\ C_j \\ C_k \\ C_l \end{pmatrix} = \begin{pmatrix} f_{a1} \\ f_{b1} + f_{a2} \\ f_{b2} + f_{a3} \\ f_{b3} \end{pmatrix}$$

where C_i, C_j, C_k and C_l are the concentrations at each node and each color represents an element (delimited by the nodes i, j, k, l) and the different contributions from each element to the system of equations can be visualized.

The system obtained after projecting the problem has the same number of equations and unknowns as the dimension of the base functions space.

Note that for many finite elements, the integral of equation 3.17, which is applied for each finite element, is 0 in spaces where test and base functions do not overlap, but when they overlap, the contribution to the matrix is different from

0. Actually, the diagonal elements of the stiffness matrix are formed by the terms of the equation in which i = j, when both base functions are identical. Hence, the final system matrix is formed by equations (one per node) with a few of non-zero terms corresponding to the overlap of base functions in adjacent finite elements.

3.2.4. Error estimation

The error estimate (difference between the exact solution and the numerical one) has a big importance as the numerical approximation to the solution converges reached a certain error tolerance.[34]

The higher the number of nodes, the more finite elements created and the faster the numerical approximation converges to the exact solution; but the finer the mesh resolution, the higher computable costs are required and the longer it takes to obtain the results.[31]

An a priori error estimation consists on calculating the possible error of the mathematical model before solving the equations and then using it to predict the convergence order, which determines how the error is expected to change as the number of nodes increase; but a priori estimations of the error can only be done if the problem is simple. On the other hand, a posteriori estimate uses the solutions obtained in similar problems and compares them to the solution approximation.[34]

In order to minimize the error, some procedures can be carried out, such as increasing the mesh density in regions of the numerical domain where the solution varies fast, adapting the mesh refinement to the error of a previous solution in a time-evolving problem, or reducing the time step.[34]

3.3. FEM with FreeFem++

3.3.1. FreeFem++

FreeFem++ is a high-level integrated development environment (IDE) for numerically solving partial differential equations in 2D and 3D based on the Finite Element Method.[36]

It is a free integrated product with its own high level programming language, not a package. FreeFem++ allows to describe a problem by its variational formu-

lation, with access to internal matrices and vectors if needed; has an automatic mesh generator, capable of mesh adaptation through the execution, with a variety of triangular finite elements (linear, quadratic, discontinuous...); and provides visualizations of the meshes and the solutions of the problems. Another characteristic of FreeFem++ is that is able to deal with 2D and 3D problems with multi-variables and multi-equations for static or time dependent, linear or non-linear coupled systems.[36]

3.3.2. Simulation of the 1D pressure driven flow through air diffusion in PDMS

In this section the structure of a FreeFem++ script will be explained including how to define a problem in FreeFem++ language. The following example is a script for the simplest problem that has been solved, a 1D simulation of the PDMS pumping performance explained in section 2.

```
1  //  Boundary definition
2  real h = 1.;
3  border a1(t=0,1){ x=t; y=0; label=1;}
4  border a2(t=0,h){ x=1; y=t; label=2;}
5  border a3(t=0,1){ x=1-t; y=h; label=3;}
6  border a4(t=0,h){ x=0; y=h-t; label=4;}
7  //  Mesh Th generation
8  mesh Th= buildmesh(a1(80)+a2(40)+a3(80)+a4(40));
9  //  Finite element space Vh over Th, P1
10 fespace Vh(Th,P1);
11 //  Definition of u and v as piecewise-P1 continuous functions
12 Vh   uh, vh, uh0=0.;
13 //  Constants needed
14 real omegah = 0.2732;
15 real omegac = 2.443e-4;
16 real bbeta = 0.169;
17 real ue = 1.-omegac;   //  BC at wall 1
18 real eta=0., p=omegac; //  Params to define pressure
19 real deta;             //  eta derivative
20 real dt=1e-4, Tf=3.5;  //  Params relative to the time marching
21 real dphi;             //  Mass flux across the interface
22
23 ofstream file("freefem_simulation.dat");
24
25 //  Define the gradient of a scalar field
26 macro Grad(u)[dx(u),dy(u)]
27
28 //  Diffusion equation in PDMS stated in its variational form,
     equation 3.4
```

```
29 problem pdmsdiffusion(uh,vh) = int2d(Th)(uh*vh/dt +  Grad(uh)'*
       Grad(vh)) - int2d(Th)(uh0*vh/dt) + on(1,uh=ue);
30
31 int kk=0; // Counter
32
33 uh = uh0; // Initial condition
34
35 //  Main program loop
36 for (real t=0.;t<Tf;t+=dt) {
37
38     ue = 1.-p;  // Equation 2.23
39     //  Compute uh at the next time step
40     pdmsdiffusion;
41     //  The new initial condition is the solution just obtained
42     uh0 = uh;
43
44     //  Plot the scalar field uh
45     if ( !(kk % 100))
46         plot(uh,cmm="t="+t+"[sec]",dim=2,fill=true,value=true);
47         file << t+dt+" "+dphi+" "+eta+" "+p+"\n";
48         cout << t+dt+" "+dphi+" "+eta+" "+p+"\n";
49         // Adapts mesh to optimize the execution time by adding
               and removing nodes where necessary
50         Th = adaptmesh(Th,uh,err=0.005);
51     kk+=1;
52
53     //  Define the flux at surface 1, equation 2.15
54     dphi = -bbeta*int1d(Th,1)(dx(uh)*N.x + dy(uh)*N.y);
55
56     deta = -dphi/(omegah*(1.-2.*eta)+ 1. - omegac); // Eq. 2.18
57     eta  = eta + dt*deta;
58     p    = omegah*eta + omegac; // Eq. 2.14
59 }
```

The problem has been set in its variational form in line 29 (equation 3.4). In FreeFem++ bilinear and linear terms should not be under the same integral [36]. The boundary conditions are set through the labels of the boundaries defined at the beginning of the script. Boundary condition in line 38 corresponds to equation 2.23; ϕ' definition, in line 54, corresponds to the molar flux in 2.15; η', in line 56, to 2.18; η, in line 57, is integrated by finite differences; and $\tilde{P}$, in line 58, defined in 2.14 neglecting Ω_d given its small order of magnitude. Note that in line 50 the mesh becomes adapted, nodes are added or removed where necessary to optimize the execution computational time and efforts.

The rest of scripts used for the simulations generated are equal but they have a higher complexity either in terms of geometry or equations such as the pressure term inside the empty hole of some PDMS structures or the integrals.

The way to ensure that the solution of each simulation had converged was to refine the mesh and reduce the time step and compare the results obtained until the solutions were equal. The mesh refinement and time step chosen were those able to provide a solution which converged but under the minimum computational costs.

4. RESULTS AND DISCUSSION

Although the main objectives of the project are the physical description of the PDMS pump and the development of a tool to simulate it's working mechanism and not the characterization of different structures for concrete applications, the study of certain geometrical effects has been performed to show how useful the tool is. The evolution of the pressure, the wetted length and the molar flux to the PDMS slab are analyzed for different PDMS slab geometries. The effect of two geometric features was proposed by the UPV microfluidics team to be studied. The first suggested geometry to model was an empty hole in the interior of the PDMS slab and, the second, a slab with embedded spikes at the free surface, both expected to have an effect in the molar flux and, therefore, in the pumping rate. Regarding the first structure it has been studied the effect of introducing sticks in the cubic hole, the position of the hole with respect to the face in contact with air and, also, the volume of the hole; and with respect to the sticks, simulations for different sticks height have been generated.

Firstly, a 1D simulation has been performed to validate the solution of FEM obtained with FreeFem++ with the analytical one and the one of finite differences obtained with Matlab. Then, 2D simulations have also been generated to study some effects in the geometry in a qualitative way since the exact solution cannot be obtained with two dimensional simulations. Finally, 3D simulations have also been performed both through 2D simulations in cylindrical coordinates, whose solution is yet 3D for axisymmetric geometries, and 3D simulations with actual 3D meshes. The advantage of performing simulations in cylindrical coordinates with respect to 3D simulations itself is that apart from generating simpler geometries, the computational cost of simulations in cylindrical coordinates is much less.

Note that all the simulations have an initial pressure in the PDMS of 0, this means, no air exists in the slab; and all the PDMS slabs have all their surfaces covered by epoxy glue except from one, the free surface. Screenshots of the time-evolving field (simulations) have been taken at dimensionless times between $\tau = 0.25$ and $\tau = 1$ and are shown in this section in order to visualize the different geometries used. In the structures of the screenshots, the free surface in contact with air is the one below; in axisymmetric geometries, the axis is situated at the left side; and each colour represents a region with a certain range of air concentration.

To perform the simulations the values in table 6.2 have been used, which are those used to explain the physics in section 2. All the graphs except the ones in

section 4.2 show the dimensionless pressure variation, wetted length and molar flux vs. time.

The dimensionless time step used to solve the problem both in FreeFem++ and with finite differences in 1D is 0.001. For the rest of simulations made with FreeFem++ in 2D and 3D, the time step has not been reduced more than 10^{-4}. All the simulations except those in section 4.8 had an execution time no longer than 15 minutes since during execution the mesh was being adapted situating and removing nodes were needed. However, those simulations in section 4.8 took several hours to be performed as apart from not adapting the mesh, they are 3D simulations whose computational costs are much higher.

4.1. Validation of solutions

4.1.1. Analytical, finite differences and FEM 1D Diffusion of air into a PDMS slab in an open system

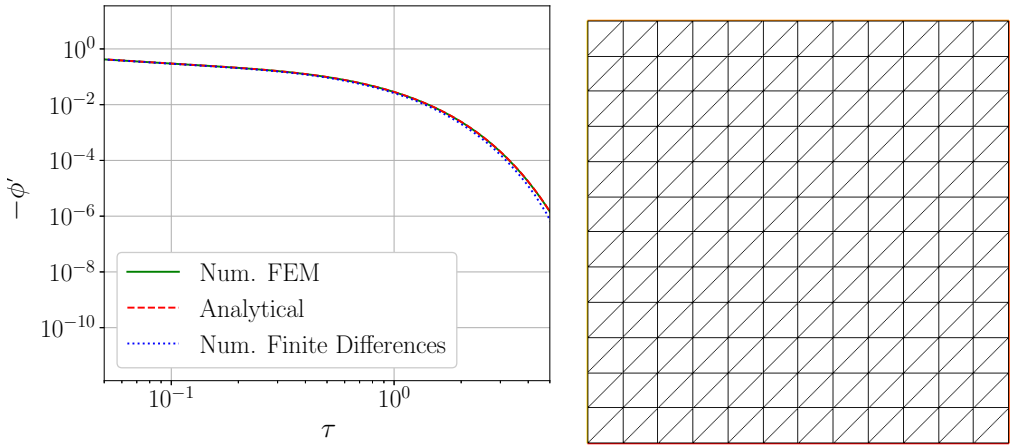

(a) Simplest diffusion problem molar flux analytical solution and solutions obtained through finite differences and FEM.

(b) Triangular mesh generated in FreeFem++ to solve the 1D diffusion problem.

Fig. 4.1. 1D analytical solution, finite differences, FEM.

Solutions for a 1D problem in which air diffuses into a PDMS slab with every surface coated with epoxy resin except from one, but with no fluid pumped, have been obtained in a theoretical manner, through finite differences (implemented in Matlab) and with FEM (in a FreeFem++ simulation). The molar flux vs. time plot of all of them is shown in figure 4.1.a, where it can be observed the three solutions are equal, validating FreeFem++ as the differential equation solver to be used to simulate the

pumping process for different PDMS geometries.

The mesh used in FreeFem++ is shown in the figure 4.1.b, with dimensionless domain of 1×1; while the mesh used for the finite differences is the one shown in figure 2.2, where the dimensionless domain of length 1 is discretized in 100 points. The meshes for 2D and 3D simulations have been much more refined that the one shown here (4 or 5 times). However, most of them have been automatically adapted.

4.1.2. Finite differences vs. FEM 1D Diffusion of air into a PDMS slab in a closed system for driving fluid

The following graphs show the variation of pressure, wetted length and molar flux evolutions, obtained both with finite differences and with FEM (FreeFem++), in the closed system of figure 2.1, in which a fluid is being pumped through the negative pressure generated after air diffusion into PDMS. The comparison between both solutions represents a second validation for the FreeFem++ simulations since the problem solved is a more complex one than the solutions in section 4.1.1, where a flow is not being driven.

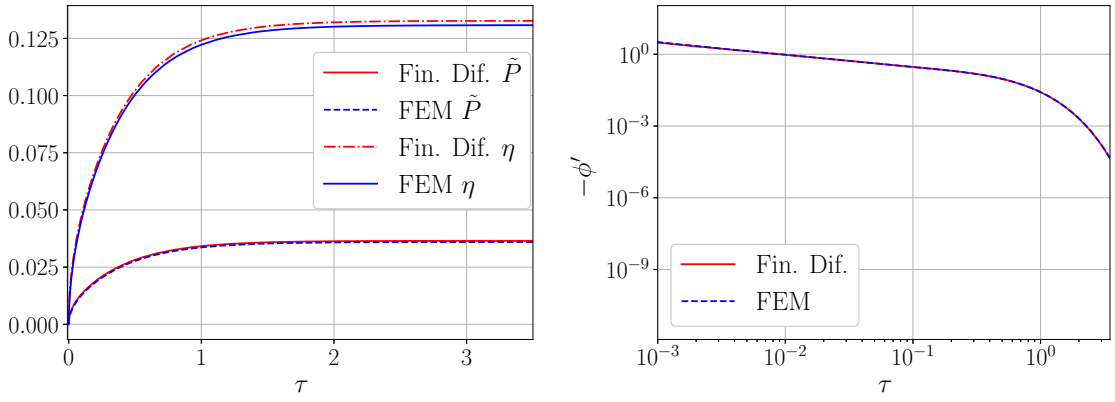

(a) Dimensionless pressure and wetted length vs. time.

(b) Log plot of dimensionless molar flux vs. time.

Fig. 4.2. 1D solution finite differences vs. FEM.

4.2. FEM 1D diffusion of air into a PDMS slab in a closed system for driving fluid

The following graphs show the time evolution of the pressure variation, the wetted length and the molar flux through the PDMS obtained through a 1D simulation

with FreeFem++ (for the system shown in figure 2.1).

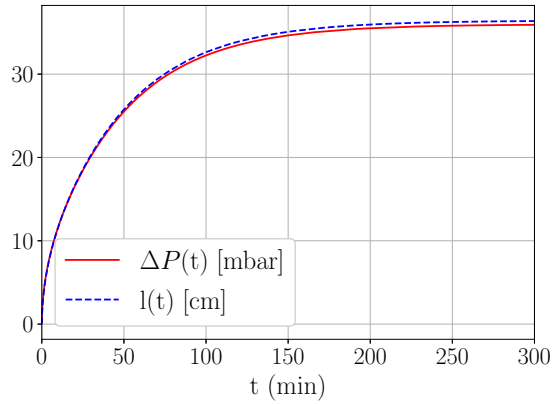

(a) Pressure variation and wetted length vs. time.

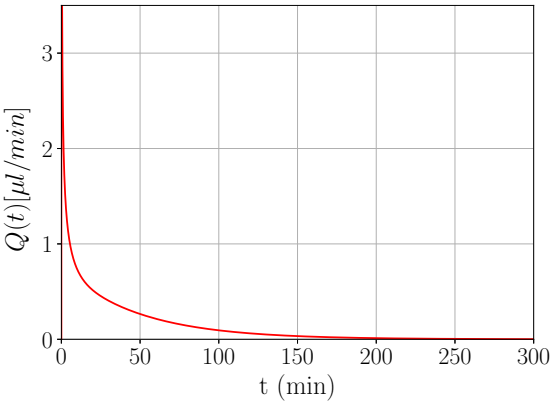

(b) Molar flux vs. time.

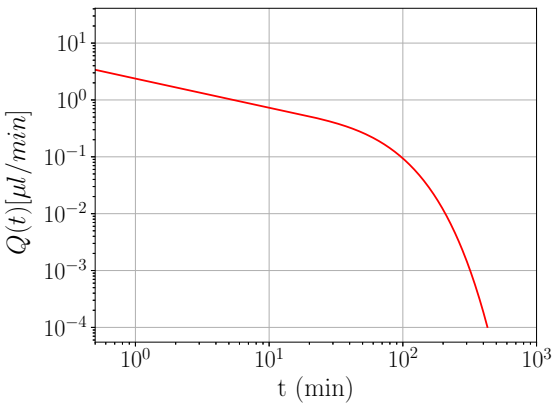

(c) Log plot of molar flux vs. time.

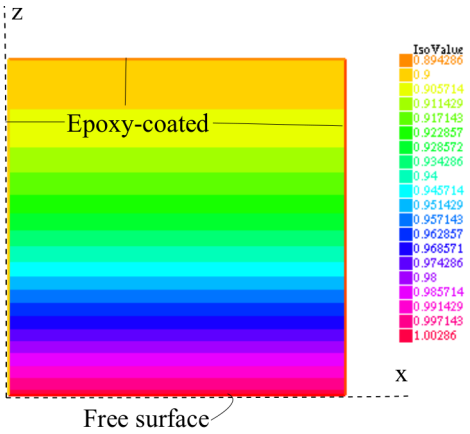

(d) 1D diffusion simulation with FreeFem++.

Fig. 4.3. 1D solution with FEM (FreeFem++).

4.3. Effect of an empty hole in the interior of the PDMS slab

To study the effect of an empty hole in the interior of the PDMS slab both 2D and 3D (axisymmetric) solutions have been obtained. The 3D axisymmetric simulation has been performed through a 2D formulation of the problem in cylindrical coordinates. To develop the problem formulation in FreeFem++, section 2.6.2 has been taken as reference for the physical description. The 2D simulations correspond to a cube with a transverse hole that goes from the front wall of the cube to the back wall and the axisymmetric simulations correspond to a cylinder, both solid and with a hole in its interior, whose axial cut is represented in figure 4.7, with axis on the left side. Note that the 2D simulation has a hole volume much bigger than the 3D

axisymmetric simulation.

2D solution

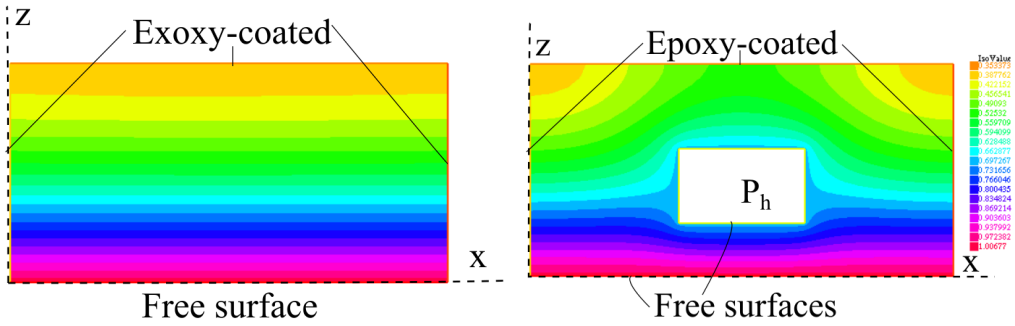

Fig. 4.4. 2D simulations in FreeFem++ for slabs without and with an interior hole.

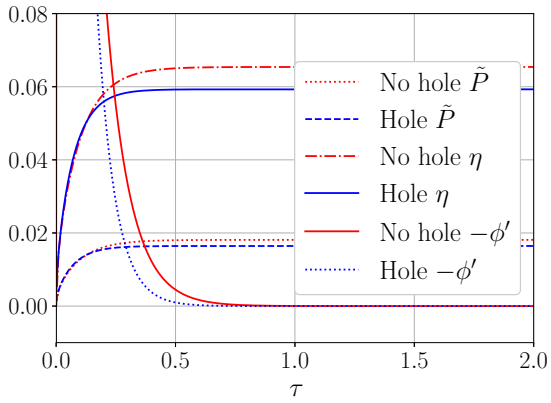

(a) Dimensionless pressure variation and wetted length vs. time.

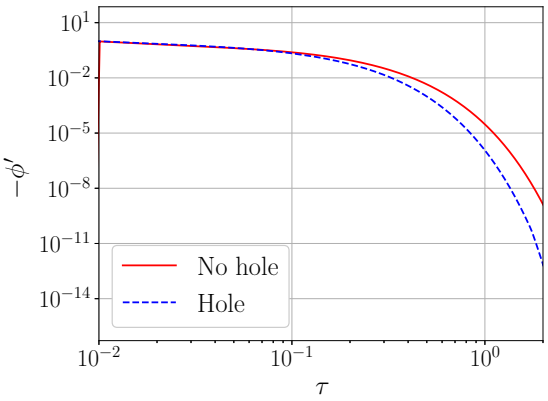

(b) Dimensionless molar flux vs. time.

Fig. 4.5. Diffusion of air into both a solid PDMS slab and a PDMS slab with a hole (2D solution).

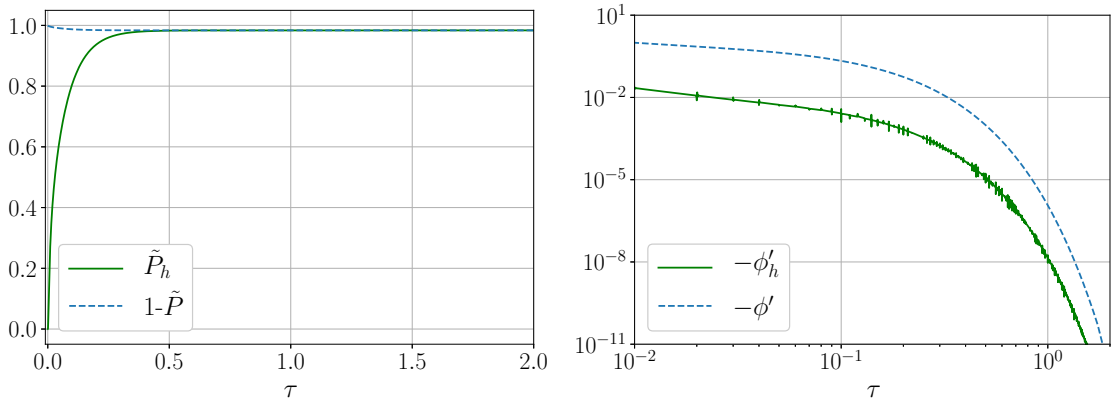

(a) Dimensionless variation of pressure inside the hole and 1 - variation of pressure in the channel vs. time.

(b) Dimensionless molar flux in the hole and in the free surface vs. time.

Fig. 4.6. Pressure and molar flux in the hole (2D solution).

3D axisymmetric solution

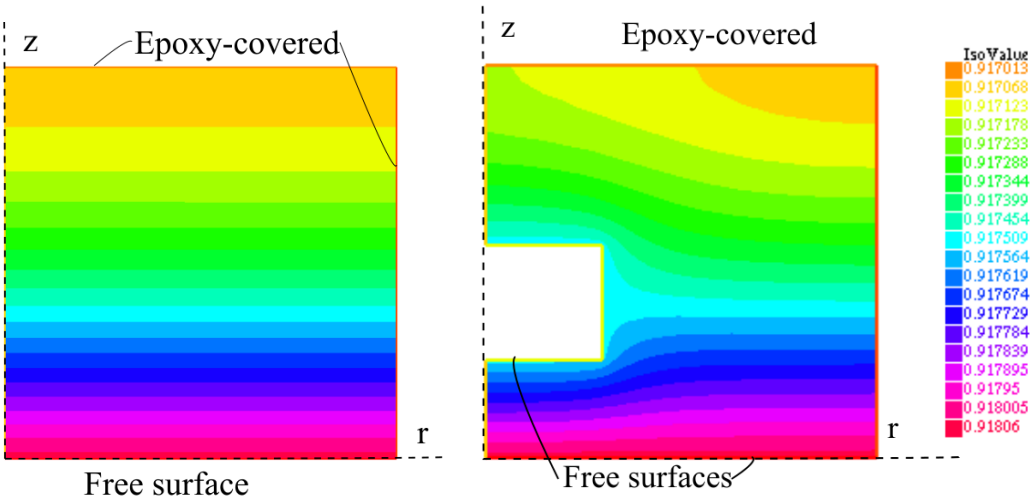

Fig. 4.7. 3D axisymmetric simulations in FreeFem++ for slabs without and with an interior hole.

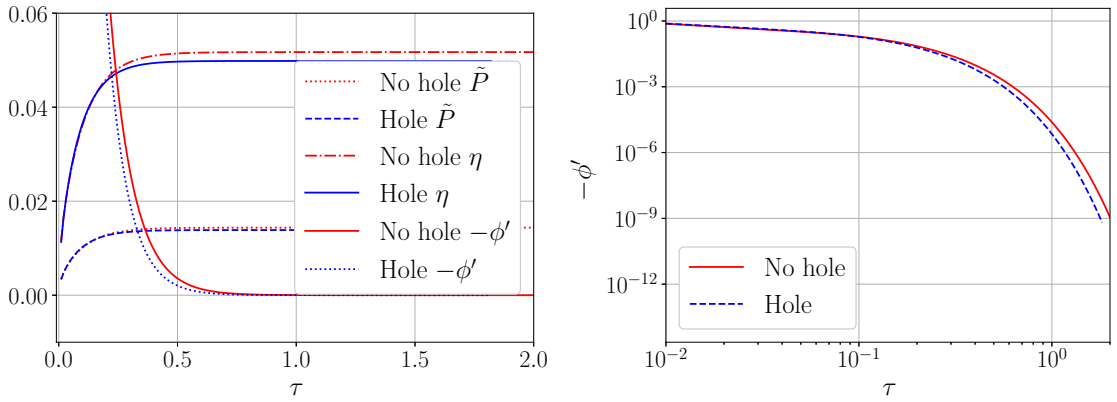

(a) Dimensionless pressure variation and wetted length vs. time.

(b) Dimensionless molar flux vs. time.

Fig. 4.8. Diffusion of air into both a solid PDMS slab and a PDMS slab with a hole (axisymmetric 3D solution).

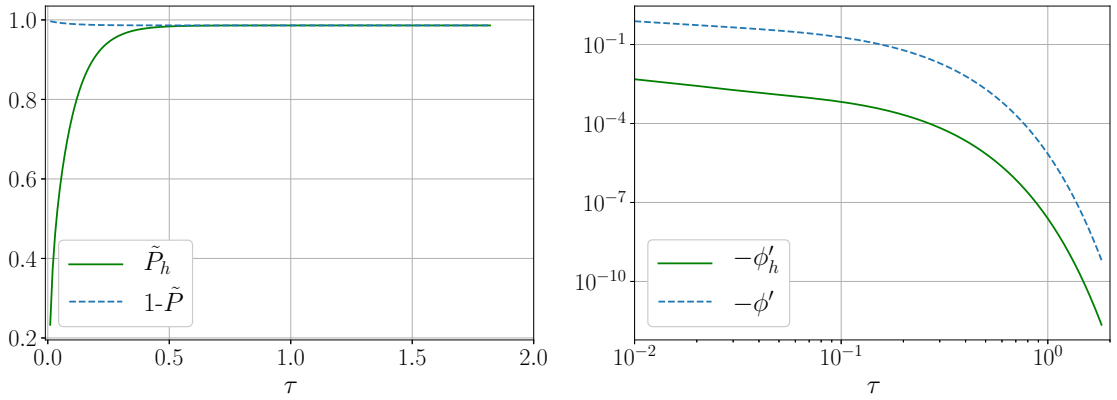

(a) Dimensionless variation of pressure inside the hole and 1 - variation of pressure in the channel vs. time.

(b) Dimensionless molar flux in the hole and in the free surface vs. time.

Fig. 4.9. Pressure and molar flux in the hole (3D axisymmetric solution).

Up to certain moment the graphs of both geometries in 2D and 3D are equal since the hole has no effect until the air reaches it. When it does, it can be observed that introducing an empty hole in the slab decreases the pressure drop, consequent wetted length and the molar flux through the free wall. This effect is more pronounced in the 2D simulation since the volume of the hole is bigger than in the 3D axisymmetric geometry. The effect of introducing a hole can help to avoid pulses in the flow.

Note that when equilibrium is reached and no more mass flux exists, the dimensionless variation of pressure outside the slab and the dimensionless variation of pressure inside the hole sum 1.

4.4. Effect of sticks in the empty hole in the interior of the PDMS slab

The effect of placing sticks in the interior of the hole has also been studied since this is the actual geometry being used by the UPV team for their initial experiments. However, the simulations performed have both been performed in 2D and axisymmetric and none of them show a big effect in the pressure variation, wetted length or molar flux. The results are consistent with the ones obtained in section 4.3, where the effect of the empty hole was shown to reduce the pressure variation, wetted length and molar flux. This can be observed in graphs 4.11 and 4.13 since the introduction of sticks that make the empty volume of the hole bigger make the pressure variation, wetted length and molar flux decrease.

2D solution

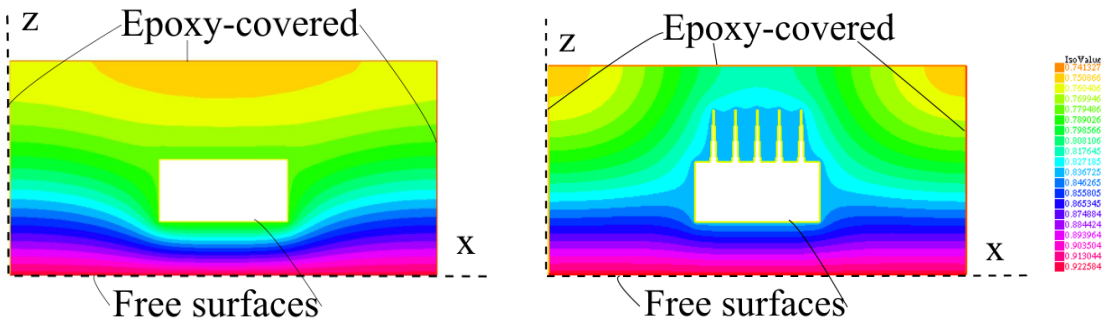

Fig. 4.10. 2D simulations in FreeFem++ for slabs with an interior hole with and without sticks.

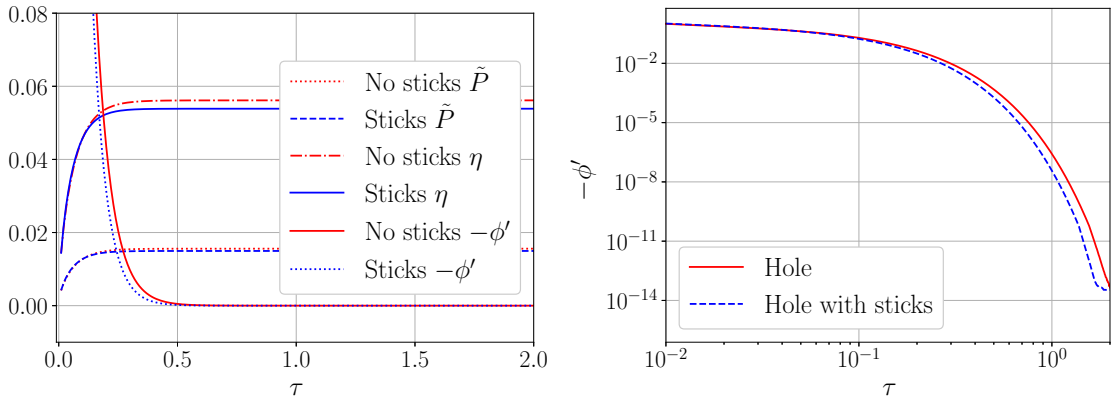

(a) Dimensionless pressure variation, wetted length and molar flux vs. time.

(b) Dimensionless molar flux vs. time.

Fig. 4.11. Diffusion of air into both a PDMS slab with a hole and a PDMS slab with a hole with sticks 2D simulation.

3D axisymmetric solution

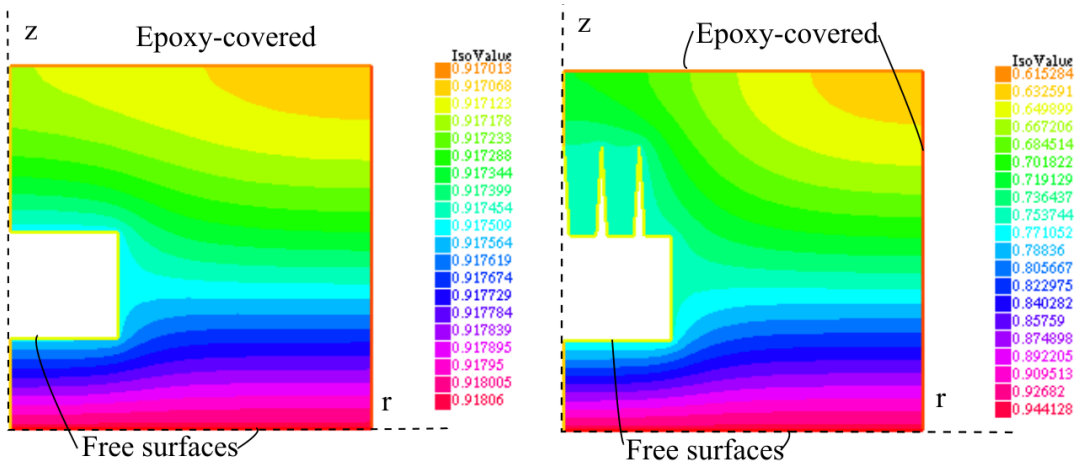

Fig. 4.12. Axisymmetric 3D simulations in FreeFem++ for slabs with an interior hole with and without sticks.

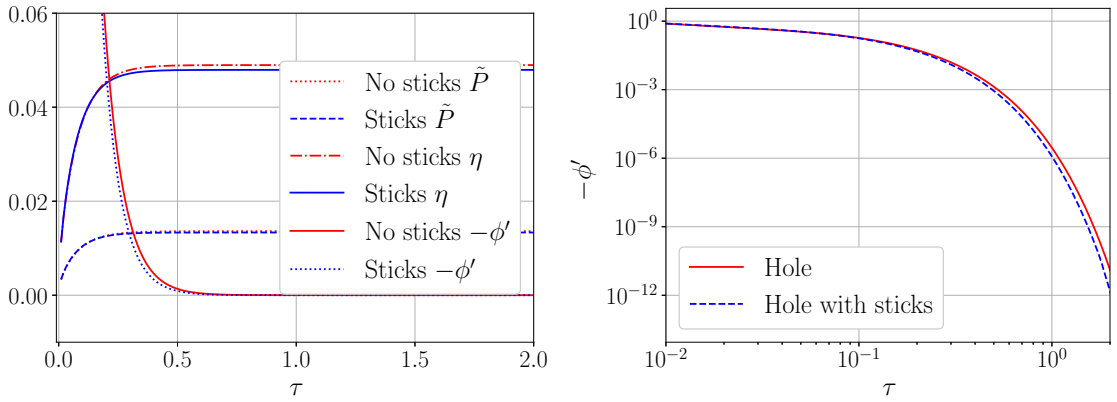

(a) Dimensionless pressure variation, wetted length and molar flux vs. time.

(b) Dimensionless molar flux vs. time.

Fig. 4.13. Diffusion of air into both a PDMS slab with a hole and a PDMS slab with a hole with sticks 3D axisymmetric simulation.

4.5. Effect of the volume of the empty hole in the interior of the PDMS slab

Although in section 4.4 it has been shown that the bigger the hole volume, the more the pressure variation, wetted length and molar flux become reduced, in this section 3D axisymmetric simulations have been performed for different hole volumes and graphs 4.15 confirm this conclusion again. Increasing the volume of the empty hole in the PDMS slab decreases the total pumping capacity, this means, the net wetted length the fluid is moved becomes reduced since the total amount of PDMS decreases for a same sized slab.

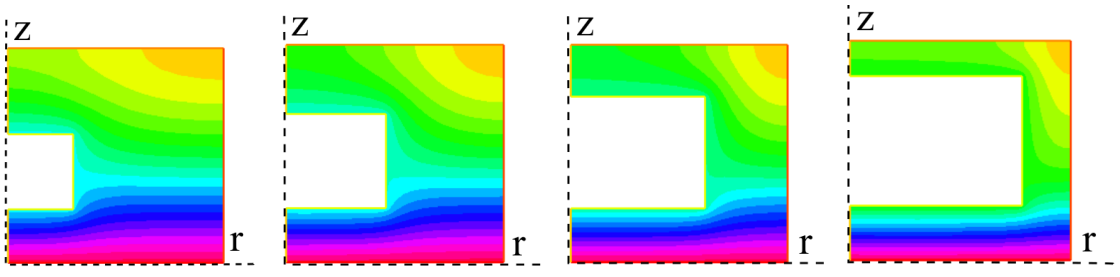

Fig. 4.14. Axisymmetric 3D simulations in FreeFem++ for slabs with an interior hole of different volumes. The total slab volume including the hole is of $500mm^3$.

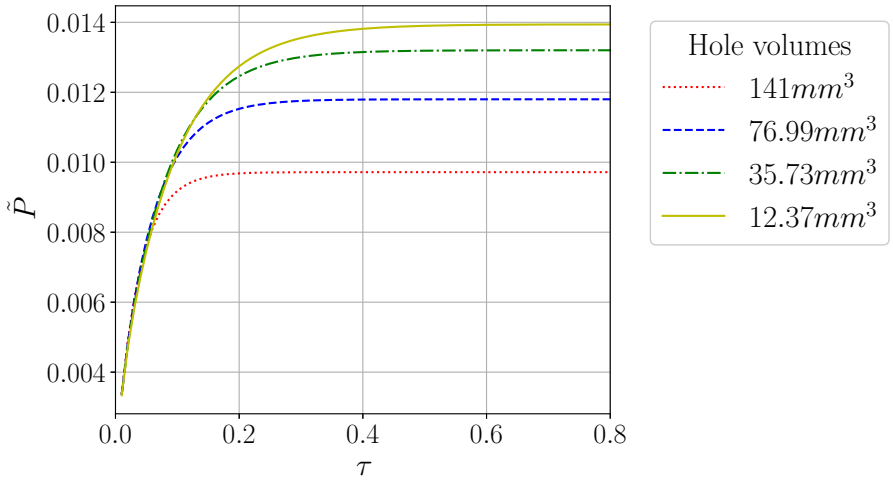

(a) Pressure variation vs. time

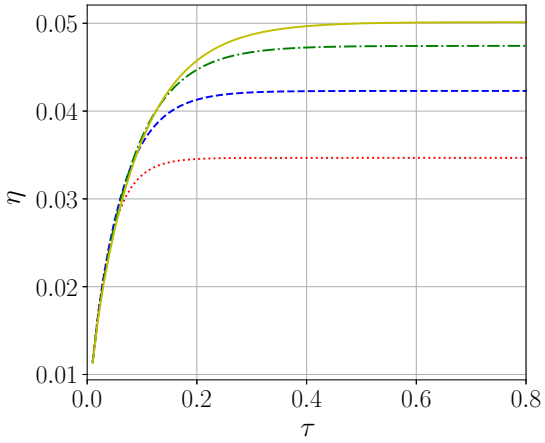

(b) Wetted length vs. time

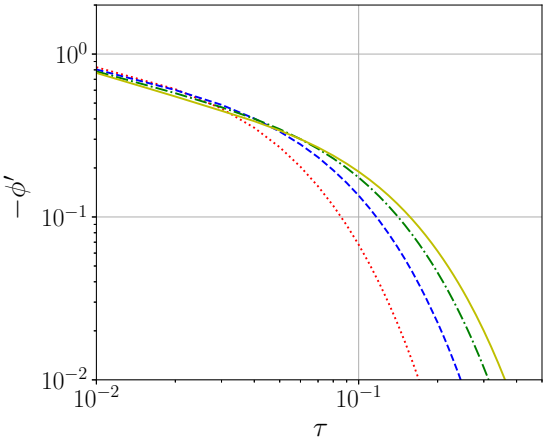

(c) Log plot of molar flux vs. time

Fig. 4.15. Solution for different volumes of the hole in the PDMS slab (axisymmetric 3D simulations).

4.6. Effect of the position of an empty hole in the interior of the PDMS slab

3D axisymmetric simulations for equal volume holes situated at different distances from the free surface of the PDMS slab have been performed. It can be observed that the closer the hole is to the wall in contact with air, the sharper is the pressure drop, the higher is the air flux to the PDMS and the steeper is the pulse of flow generated. Therefore, since the PDMS volume is equal for all geometries, the effective pumping time is smaller than for geometries with a hole farther from the free surface.

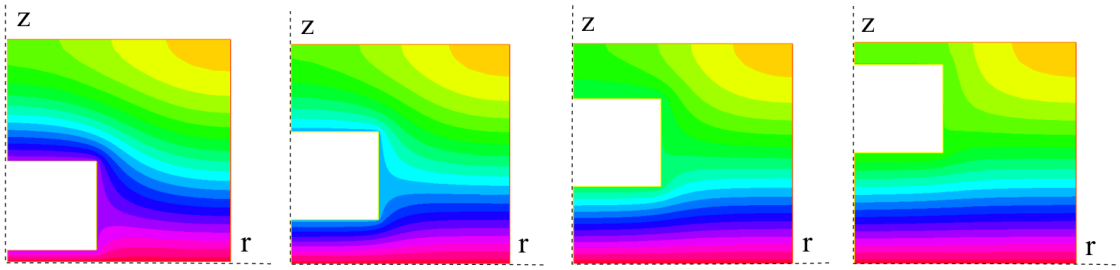

Fig. 4.16. Axisymmetric simulations in FreeFem++ for slabs with an interior hole at different positions.

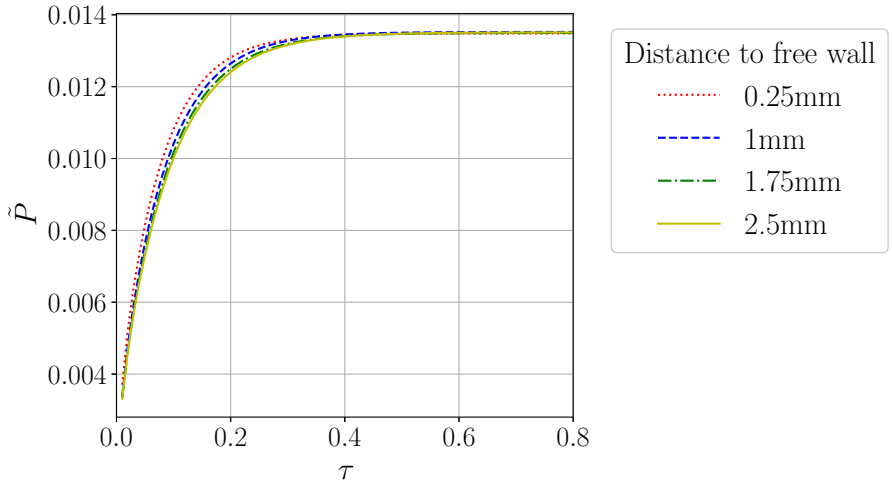

(a) Pressure variation vs. time

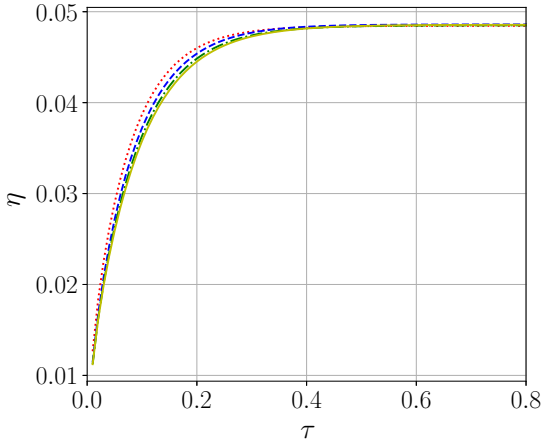

(b) Wetted length vs. time

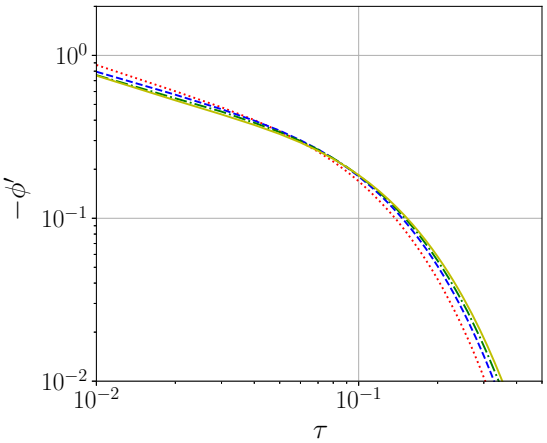

(c) Log plot of molar flux vs. time

Fig. 4.17. Solution for different positions of the hole in the PDMS slab (axisymmetric 3D simulations).

4.7. Effect of the height of the sticks in the free surface of a PDMS slab

2D simulations have been performed for different PDMS slabs with embedded spikes of different heights on its free surface. These results are consistent with the parameters that affect the pumping perfomance in section 1.3.2 as the pressure increases with the increase of surface area and the total driving pressure drop with the volume. The taller the sticks, the steeper is the pressure drop and the molar flux increases but the total pressure variation and wetted length of the fluid become reduced since the less volume is occupied by PDMS.

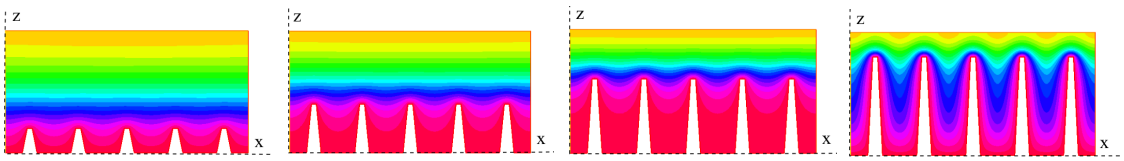

Fig. 4.18. 2D simulations in FreeFem++ for slabs with embedded sticks of different height.

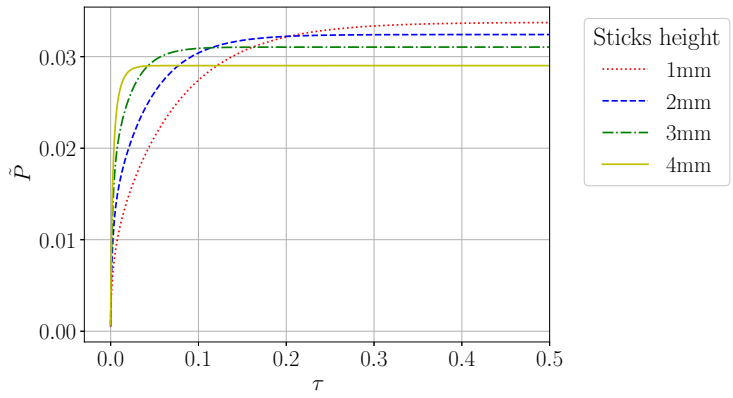

(a) Pressure variation vs. time.

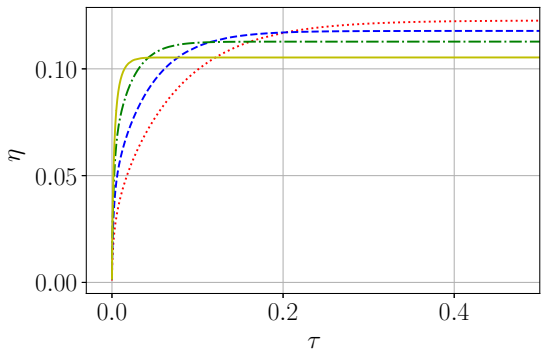

(b) Wetted length vs. time.

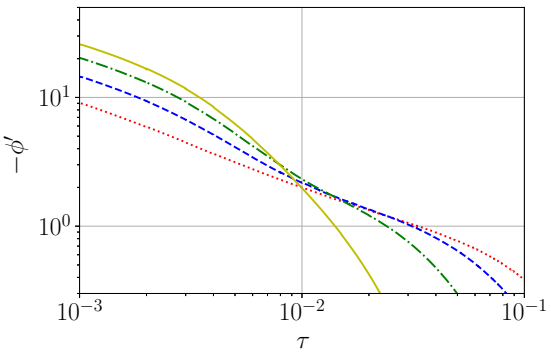

(c) Log plot of molar flux vs. time.

Fig. 4.19. Solution for different heights of sticks in the PDMS slab (2D simulations).

4.8. Effect of an embedded cube at the free surface and an embedded cube with sticks

3D geometries where generated with GMSH and used for the 3D FreeFem++ simulations.

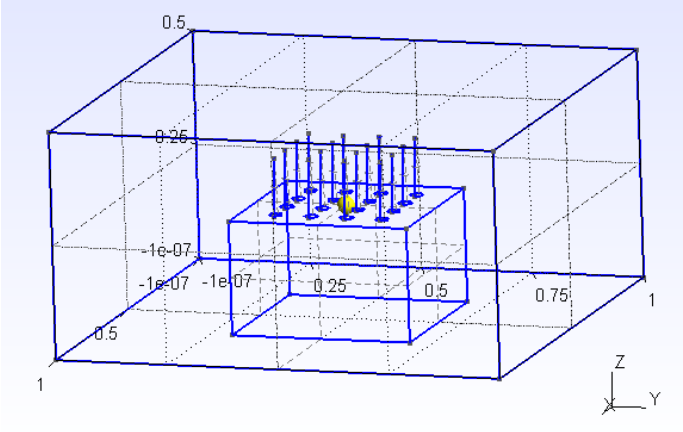

Fig. 4.20. Cube with embedded cube with embedded sticks at the free surface.

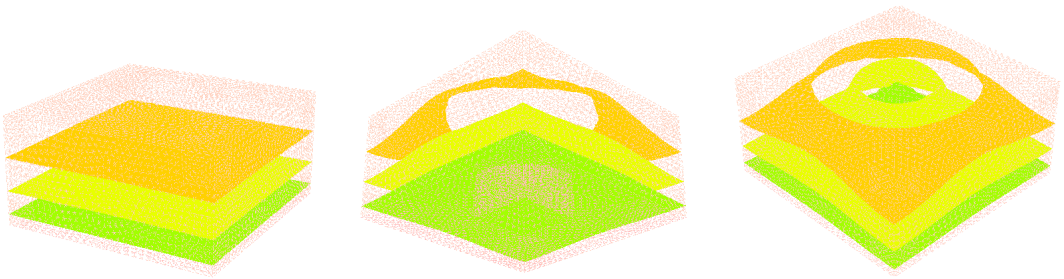

(a) Cube.

(b) Cube with embedded cube at the free surface.

(c) Cube with embedded cube with embedded sticks at the free surface.

Fig. 4.21. 3D simulations in FreeFem++ for slabs with different geometries.

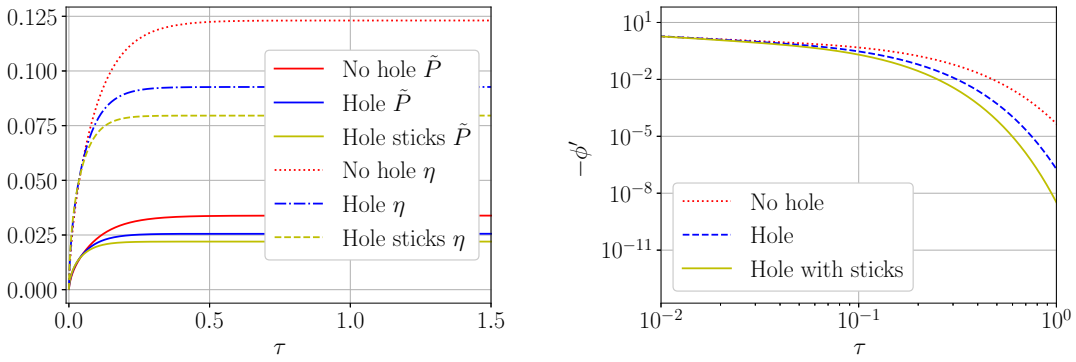

(a) Dimensionless pressure variation and wetted length vs. time.

(b) Dimensionless molar flux vs. time.

Fig. 4.22. Diffusion of air into slabs with different geometries (3D simulations).

Results in figure 4.22 show that the more PDMS pump volume, the bigger pressure drop is obtained and the longer the fluid becomes moved, consistent with results in previous sections. However, an increase in the molar flux was also expected when introducing an embedded smaller cube in the free surface of a cube and even more if it had embedded spikes also (because the surface in contact with air is larger), but a rapid air saturation of the slab only resulted in a decrease of the flux. Therefore, to increase more the molar flux through the free surface it would be better to use geometries with just embedded spikes as the shown in section 4.7.

5. CONCLUSIONS AND FURTHER STEPS

In this project the working mechanism of the PDMS pressure-driven pump has been physically modeled and simulated with FEM for the different proposed geometries by the UPV microfluidics research team. Given the importance of flow control in microfluidic devices for many different applications, the geometries to model were expected to have an effect in the pressure drop and consequent molar flux. Simulations of the degassed-driven flows for different PDMS structures provide approximations of the desired conditions without the need of making experiments and, therefore, a better study of influencing parameters, saving time and money.

The results obtained in the simulations for different geometries have shown to be consistent with the results reported in the literature[2] and explained in section 1.3.2. The higher the area in contact with air, the more pumping pressure and molar flux and the smaller is the effective pumping period since the PDMS slab gets full of gas sooner; and the bigger the slab, the more air can be absorbed, the bigger the pressure variation, wetted length, molar flux and time it takes for the pumping performance to end.

Regarding the concrete proposed geometries it has been shown that the presence of an empty hole in the interior of the PDMS slab reduced the pressure drop the same manner a smaller slab would do. The effect of the hole only adds value to the effect of reducing the PDMS slab size to control the molar flux for equal pressure drops and net wetted lengths by varying the position of the hole in the slab. Furthermore, although the results obtained with the introduction of sticks in the hole do not provide a different effect than just varying the hole volume, a further study could be performed in a future for different hole geometries, like for different spacing between the sticks, with expected effects in the resulting molar flux. Therefore, by combining different PDMS slabs with different geometries (with or without hole or different hole volumes or shapes), different pumping curves would be obtained for different applications. Finally, from sections 4.7 and 4.8 it can be concluded that increasing the molar flux and making the pressure drop steeper can be performed in a more effective manner by using geometries where the surface is increased in a way saturation of PDMS does not happen easily, as with the introduction of embedded spikes in the free surface (4.7), instead on an embedded cube (4.8). These results show how useful the developed simulating tool is for the design of different PDMS pumps depending on the application.

The next steps to follow in order to characterize the PDMS pumping mechanism,

that will be performed by the collaborators of UPV, are the experimental validation of the numerical solutions and a further simulation process to better identify and understand geometric parameters with effect in the fluid flow.

However, the main problem of FreeFem++ is the meshing tool it provides to define 3D meshes. In order to make relatively complex geometries, GMSH has been used but still it is not a user-friendly program at all. Solutions for 2D and 3D axisymmetric geometries can be easily obtained with the meshing algorithm FreeFem++ provides but not for 3D complex structures. Therefore, given the difficulty to generate 3D meshes, regarding providing a user with no engineering background with a product to simulate the PDMS pumping performance, the recommendation to model complex PDMS structures would be to use a commercial software such as Comsol and, hence, the objective of the project which is providing to UPV team with an easy to use simulating tool would not be satisfied unless another appropriate meshing program compatible with FreeFem++ were found.

Nevertheless, the present work has described a pumping mechanism based on the PDMS permeability and solubility for microfluidics in BioMEMS which meets the requirements of being simple, requiring small energy inputs and allowing a precise control over the flows. This represents a very suitable solution for the current problem of fulfilling this demands in BioMEMS or LOC devices.[20][1][2] So, to conclude, after a further research process, PDMS based pumps could be used in many microfluidics applications with successful results.

6. BUDGET

The budget of the project has consisted on the engineering work, the software costs and the computer depreciation cost. The contribution of Matlab to the costs could already have been saved since the 1D part implemented in Matlab could have been done with free software like Python. All the postprocessing of results data has actually been performed with Python.

- Junior engineering salary = 6.25 €/ hour × 350 hours = 2187.5 €[39]
- Matlab student license = 35 €[40]
- Computer depreciation cost = (total cost/total life hours) × hours in project = (600 €/ (7 years × 365days/year × 3 hours/day) × 350 hours = 27 €

Engineering work	2187.5 €
Matlab license	35 €
Computer depreciation cost	27 €
Total costs	2249.5 €

Table 6.1. Total costs

It is also remarkable to note the savings of using the free tools FreeFem++ and GMSH for the Finite Element models instead of the mainly used Comsol.
Comsol Fluid Module Class Kit License = 2578 €.[41]

BIBLIOGRAPHY

[1] L. Xu, H. Lee, D. Jetta, and K. W. Oh, "Vacuum-driven power-free microfluidics utilizing the gas solubility or permeability of polydimethylsiloxane (pdms)," *Lab On A Chip*, vol. 15, pp. 3962–3979, 20 2015. DOI: 10.1039/C5LC00716J.

[2] G. Li, Y. Luo, L. Liao, and J. Zhao, "A "place n play" modular pump for portable microfluidic applications," *Biomicrofluidics*, vol. 6, 2012. DOI: 10.1063/1.3692770.

[3] R. R. Jivani *et al.*, "Biomedical microelectromechanical systems (biomems): Revolution in drug delivery and analytical techniques.," *Saudi pharmaceutical journal : SPJ : the official publication of the Saudi Pharmaceutical Society*, vol. 24, pp. 1–20, 1 2016.

[4] S. Haeberle and R. Zengerle, "Microfluidic platforms for lab-on-a-chip applications.," *Lab on a chip*, vol. 7, pp. 1094–110, 9 2007. DOI: 10.1039/B706364B.

[5] S. Lee and S. Lee, "Micro total analysis system (micro-tas) in biotechnology.," *Applied microbiology and biotechnology*, vol. 64, pp. 289–99, 3 2004.

[6] Wikipedia contributors, *Bio-mems — Wikipedia, the free encyclopedia*, [Online; accessed 14-September-2018], 2018. [Online]. Available: https://en.wikipedia.org/w/index.php?title=Bio-MEMS&oldid=858793431.

[7] A. Folch, *Introduction to BioMEMS*, 1st ed. CRC Press, Aug. 2012.

[8] B. Yao *et al.*, "A microfluidic device based on gravity and electric force driving for flow cytometry and fluorescence activated cell sorting," *Lab on a Chip*, vol. 4, pp. 603–607, 6 Nov. 2004. DOI: 10.1039/B408422E.

[9] G. M. Walker and D. J. Beebe, "A passive pumping method for microfluidic devices," *Lab on a Chip*, vol. 2, pp. 131–134, 3 Aug. 2002. DOI: 10.1039/B204381E.

[10] E. W. K. Young and D. J. Beebe, "Fundamentals of microfluidic cell culture in controlled microenvironments," *Chem. Soc. Rev.*, vol. 39, pp. 1036–1048, 3 2010. DOI: 10.1039/B909900J. [Online]. Available: http://dx.doi.org/10.1039/B909900J.

[11] N. S. Lynn and D. S. Dandy, "Passive microfluidic pumping using coupled capillary/evaporation effects," *Lab on a Chip*, vol. 9, pp. 3422–3429, 23 Oct. 2009. DOI: 10.1039/B912213C.

[12] M. Zimmermann, S. Bentley, H. Schmid, P. Hunziker, and E. Delamarche, "Continuous flow in open microfluidics using controlled evaporation," *Lab on a Chip*, vol. 5, pp. 1355–1359, 12 Oct. 2005. DOI: 10.1039/B510044E.

[13] H. Lai and A. Folch, "Design and dynamic characterization of "single-stroke" peristaltic pdms micropumps," *Lab on a Chip*, vol. 11, pp. 336–342, Oct. 2011. DOI: 10.1039/C0LC00023J. [Online]. Available: http://dx.doi.org/10.1039/C0LC00023J.

[14] X. Wang, J. A. Hagen, and I. Papautsky, "Paper pump for passive and programmable transport," *Biomicrofluidics*, vol. 7, 1 Feb. 2013. DOI: 10.1063/1.4790819.

[15] M. Zimmermann, H. Schmid, P. Hunziker, and E. Delamarche, "Capillary pumps for autonomous capillary systems," *Lab on a Chip*, vol. 7, pp. 119–125, 1 Oct. 2006. DOI: 10.1039/B609813D.

[16] C. K. Harnett, J. Templeton, K. A. Dunphy-Guzman, Y. M. Senousya, and M. P. Kanouff, "Model based design of a microfluidic mixer driven by induced charge electroosmosis," *Lab on a Chip*, vol. 8, pp. 565–572, 4 Feb. 2008. DOI: 10.1039/B717416K.

[17] D. Fine *et al.*, "A low-voltage electrokinetic nanochannel drug delivery system," *Lab on a Chip*, vol. 11, pp. 2526–2534, 15 Jun. 2011. DOI: 10.1039/C1LC00001B.

[18] X. Wang, C. Cheng, S. Wang, and S. Liu, "Electroosmotic pumps and their applications in microfluidic systems," *Microfluidics and Nanofluidics*, vol. 6, 145–162, Feb. 2009. DOI: 10.1007/s10404-008-0399-9. [Online]. Available: https://doi.org/10.1007/s10404-008-0399-9.

[19] W. S. Low, N. A. Kadri, and W. A. B. bin Wan Abas, "Computational fluid dynamics modelling of microfluidic channel for dielectrophoretic biomems application," *The Scientific World Journal*, vol. 2014, Jul. 2014. DOI: 10.1155/2014/961301. [Online]. Available: http://dx.doi.org/10.1155/2014/961301.

[20] S. K. Sia and L. J. Kricka, "Microfluidics and point-of-care testing.," *Lab on a Chip*, vol. 8, pp. 1982–1983, 12 Nov. 2008. DOI: 10.1039/B817915H.

[21] J. L. Snyder *et al.*, "High-performance, low-voltage electroosmotic pumps with molecularly thin silicon nanomembranes," *Proceedings of the National Academy of Sciences*, vol. 110, 18425–18430, 46 Nov. 2013. DOI: 10.1073/pnas.1308109110.

[22] B. Jose *et al.*, "Self-powered microfluidic device for rapid assay of antiplatelet drugs," *Langmuir*, vol. 32, pp. 2820–2828, 11 2016. DOI: 10.1021/acs.langmuir.5b03540.

[23] Wikipedia contributors, *Medical research — Wikipedia, the free encyclopedia*, [Online; accessed 22-September-2018], 2018. [Online]. Available: https://en.wikipedia.org/w/index.php?title=Medical_research&oldid=856520490.

[24] D. DiPaola, "Biomems: Navigating the medical device fda approval process," *MEMS Journal*, Nov. 2012.

[25] I. O. for Standardization, *Iso 13485 – medical devices*, [Online; accessed 22-September-2018], 2018. [Online]. Available: https://www.iso.org/iso-13485-medical-devices.html.

[26] W. contributors, *Occupational safety and health administration — Wikipedia, the free encyclopedia*, [Online; accessed 22-September-2018], 2018. [Online]. Available: https://en.wikipedia.org/w/index.php?title=Occupational_Safety_and_Health_Administration&oldid=860043732.

[27] M. P. McRae, G. Simmons, and J. T. McDevitt, "Challenges and opportunities for translating medical microdevices: Insights from the programmable bio-nano-chip," *Bioanalysis*, vol. 8, 905–919, 9 May 2016. DOI: 10.4155/bio-2015-0023.

[28] S. C. George and S. Thomas, "Transport phenomena through polymeric systems," *Progress in polymeric science*, vol. 26, pp. 985–1017, 2001.

[29] P. Bogacki and L. F. Shampine, "A 3(2) pair of runge-kutta formulas," *Applied Mathematics Letters*, vol. 2, 321–325, 4 1989. DOI: 10.1016/0893-9659(89)90079-7.

[30] L. F. Shampine and M. W. Reichelt, "The matlab ode suite," *SIAM Journal on Scientific Computing*, vol. 18, pp. 1–22, 1 1997. DOI: 10.1137/S1064827594276424.

[31] D. L. Logan, *A first course in the finite element method.* 5th ed. Cengage Learning, 2011.

[32] M. G. Larson and F. Bengzon, *The Finite Element Method, Theory, Implementation, and Applications*, 5th ed. Springer Publishing Company, Incorporated, 2013.

[33] J. Reddy, *An Introduction to the Finite Element Method.* 3rd ed., ser. MCGRAW HILL SERIES IN MECHANICAL ENGINEERING. McGraw-Hill Education, 2006.

[34] C. Multiphysics®, *An introduction to the finite element method*, 2017. [Online]. Available: https://www.comsol.com/multiphysics/finite-element-method.

[35] Wikipedia contributors, *Finite element method — Wikipedia, the free encyclopedia*, [Online; accessed 14-September-2018], 2018. [Online]. Available: https://en.wikipedia.org/w/index.php?title=Finite_element_method&oldid=859188748.

[36] F. Hecht, "New development in freefem++," *Journal of Numerical Mathematics*, vol. 20, no. 3-4, pp. 251–265, 2012. DOI: 10.1515/jnum-2012-0013..

[37] L. Bers, S. Trust, and F. John, *Contributions to the Theory of Partial Differential Equations*. Ser. Annals of Mathematics Studies 32. PRINCETON UNIVERSITY PRESS, Mar. 2016, vol. 33.

[38] Wikipedia contributors, *Divergence theorem — Wikipedia, the free encyclopedia*, [Online; accessed 15-September-2018], 2018. [Online]. Available: https://en.wikipedia.org/w/index.php?title=Divergence_theorem&oldid=859189423.

[39] U. C. I. de Madrid", *Texto consolidado de la normativa por la que se regulan las retribuciones adicionales del personal docente e investigador, aprobada por el consejo de gobierno en sesiones de 4 de marzo de 2005 y 15 de abril de 2005 y modificada en sesiones de 18 de octubre de 2007, 30 de abril de 2009, 6 de octubre de 2011, 27 de febrero de 2014, 25 de febrero de 2016 y 14 de junio de 2017*, "2017". [Online]. Available: https://e-archivo.uc3m.es/handle/10016/24971#preview (visited on 09/30/2010).

[40] T. MathWorks, *Matlab pricing and licensing*, 2018. [Online]. Available: https://es.mathworks.com/pricing-licensing.html?prodcode=ML&intendeduse=student.

[41] C. Multiphysics®, *Comsol multiphysics® software price list*, 2015. [Online]. Available: http://collaborate.bu.edu/engit/Comsol?action=AttachFile&do=get&target=comsol-pricelist.pdf.

[42] U. of Cambridge, *Finite element method: Nodes, elements, degrees of freedom and boundary conditions*, 2018. [Online]. Available: https://www.doitpoms.ac.uk/tlplib/fem/node.php.

[43] A. Universitet, *Finite element method: Nodes, elements, degrees of freedom and boundary conditions*. [Online]. Available: http://www.wind.civil.aau.dk/lecture/7sem_finite_element/lecture_notes/Lecture_1_2.pdf.

[44] E. K. Sackmann, A. L. Fulton, and D. J. Beebe, "The present and future role of microfluidics in biomedical research," *Nature*, vol. 507, 181–189, Mar. 2014. DOI: 10.1038/nature13118. [Online]. Available: http://dx.doi.org/10.1038/nature13118.

[45] A. K. Au, H. Lai, B. R. Utela, and A. Folch, "Microvalves and micropumps for biomems.," *Micromachines*, vol. 2, pp. 179–220, 2011. DOI: 10.3390/mi2020179.

[46] M. A. Eddings and B. K. Gale, "A pdms-based gas permeation pump for on-chip fluid handling in microfluidic devices.," *Journal of Micromechanics and Microengineering*, vol. 16, p. 2396, 11 2006. [Online]. Available: http://stacks.iop.org/0960-1317/16/i=11/a=021.

APPENDIX A.

Parameter	**Value**	**Units**
A	1	cm^2
H	5	mm
R	0.2	mm
V_0	350	mm^3
l_{needle}	0.05	mm
R_{needle}	2	cm
α	90	deg.
μ	1×10^{-3}	$kg\,m^{-1}\,s^{-1}$
μ_{air}	1.85×10^{-5}	$kg\,m^{-1}\,s^{-1}$
ρ	10^3	$kg\,m^{-3}$
γ	0.07	N/m
θ	92	deg.
K_h	4.86×10^{-5}	$mol/(m^3Pa)$
D	3.4×10^{-9}	m^2/s
T	293	K
P_a	10^5	Pa
g	9.81	m/s^2
R_u	8.314	J/(mol K)
$t_c = H^2/D$	120	mins
$l_c = V_0/(\pi R^2)$	2.79	m
$Q_c = V_0 D/H^2$	2.85	μl/min
$\Omega_d = 8\mu l_c^2 D/(P_a H^2)$	8.44×10^{-11}	
$\Omega_h = \rho g l_c sin\alpha/P_a$	0.2732	
$\Omega_c = 2\gamma\,\lvert cos\theta\rvert/(RP_a)$	2.443×10^{-4}	
$\beta = (K_h R_u T)(AH/V_0)$	0.169	

Table 6.2. Parameters values table for section 2

APPENDIX B.

BioMEMS	Biomedical microelectromechanical systems
LOC	Lab on a chip
μTAS	Micro total analysis systems
MEMS	Microelectromechanical systems
POC	Point of care
PDMS	Polydimethylsiloxane
UPV	Universidad del País Vasco
FEM	Finite Element Method
DNA	Deoxyribonucleic acid
FDA	Food and Drug Administration
EMA	European Medicines Agency
CE	European Conformity marking
ISO	International Organization for Standardization
UL	Underwriters Laboratories
OSHA	Occupational Safety and Health Administration
ODE	Ordinary Differential Equation
PDE	Partial Differential Equation